

NOVEL PATTERNING METHODS FOR  
FULL-COLOR POLYMER LIGHT-EMITTING  
DISPLAYS

HONGZHENG JIN

A DISSERTATION  
PRESENTED TO THE FACULTY  
OF PRINCETON UNIVERSITY  
IN CANDIDACY FOR THE DEGREE  
OF DOCTOR OF PHILOSOPHY

RECOMMENDED FOR ACCEPTANCE  
BY THE DEPARTMENT OF  
ELECTRICAL ENGINEERING

ADVISOR: JAMES C. STURM

JANUARY 2010

© Copyright by Hongzheng Jin, 2009.

All Rights Reserved

## Abstract

An important challenge for organic light-emitting diodes (OLED) manufacturing is the patterning method of the organic materials used for different colors. In this thesis, we have developed several novel patterning techniques for full-color OLED patterning.

The first method is referred to as the Large-Area Wet Micro-Printing (LAMP) method. The surface engineering techniques used to pattern the surface energy of a printing plate will be introduced. The printing setup, including parallel and registration alignment, will be discussed. Both single-color and RGB sub-pixel arrays are demonstrated. The LAMP method is a parallel process, which may have a low-cost and high-throughput potential.

The thickness of the wet-printed films is usually non-uniform. Two main approaches, a co-solvent approach and a surfactant approach, will be shown to effectively flatten the printed film. In addition, the effect of surfactant on the device performance is also studied. The use of FC-4432 surfactant is able to flatten the PVK profile without sacrificing the device performance.

The second method, transfer printing, is a dry printing method. The principle and mechanism of the transfer printing method will be discussed. RGB subpixel arrays will be demonstrated, with a color display resolution of 530 ppi. OLEDs with polymer layers printed under low temperature ( $50^{\circ}\text{C}$ ) show performance comparable to spin-coated control devices. The transfer printing method is demonstrated with very uniform film thickness with sharp edges and a very high resolution. It has a low-cost and high-throughput potential since it is a parallel process.

An alternative transfer printing method is also introduced, with the polymer layer deposited directly onto the stamp surface by spin coating. Two different approaches, a hard-hard approach and a hard-soft approach, are proposed. The hard-soft approach is shown with ability to accommodate non-uniform films. RGB subpixel arrays are demonstrated for both of the two approaches.

## Acknowledgements

I am deeply indebted to my advisor James C. Sturm, William and Edna Macaleer Professor of Engineering and Applied Science, for his support, encouragement, and invaluable guidance during the course of my Ph.D study. His exceptional insight keeps me motivated. He is always graceful while enthusiastic, which helped me at times of frustration. I can not imagine a better advisor, either from the academic or personal perspective. He is, from the bottom of my heart, the one person that is most honorable.

I would like to thank Prof. Claire Gmachl and Prof. Yueh-Lin (Lynn) Loo for taking the time to read my thesis and providing invaluable suggestions. I would also like to thank Prof. Antoine Kahn and Prof. Sigurd Wagner for serving on my thesis committee.

I thank all the members of the Sturm group at Princeton University for their help within the lab and office, these includes Min-Hao Mike Lu, Pai-hui Iris Hsu, Xiang-Zheng Bo, Rebecca Peterson, John Davis, Kun Yao, David Inglis, Keith Chung, Suberr Chi, Bahman Hekmatashoar, Weiwei Zheng, Yifei Huang, Noar Jafferis, Kevin Louthback, Jiun-yun Li and Ting Liu. I especially thank Troy Graves-Abe, Ke Long and Haizhou Yin for their help from my first days in the lab and even after their graduation. My thanks also goes to Troy and Bahman for their valuable time spent on lab maintenance. Suggestions from and discussions with Dr. Anton Darhuber, Dr. Haifeng Huang, Prof. Ghassan Jabbour, Prof. Richard Register and Prof. Yueh-Lin Loo are greatly appreciated.

I would also like to thank Helena Gleskva, Joe Palmer, Mikhail Gaevski for their great job in maintaining the clean room. In addition, I would like to thank many staff members of the Electrical Engineering Department and the PRISM for all of their help, especially to Ms Sheila Gunning, Ms Sarah Braude and Ms Carolyn Arnesen.

It was my pleasure to meet many great people in the department and throughout

the university. Special thanks to Jian Liang, Juan Gao, Zhaohui Fu, Dayi Deng, Lin Zhong, Fan Yang, Xiaogan Liang, Fengnian Xia and many more. They have made my Ph.D study a fun experience.

Through my undergraduate and master's thesis work, I am greatly indebted to my advisors Prof. Jing Zhu and Prof. Knut Urban for their guidance and instruction. Through my earlier school years, I would like to thank so many selfless advisors and teachers, without whom I could not have gone so far in my study: Dr. Xiaoyue Xiao, Ms. Lingling Zhang, Mr. Xingchang Wang and many others.

It all begun with my parents: the task to raise three of us is not easy during the hard times and you never lost your hope and had always encouraged us to pursuit higher educations. I am also greatly indebted to my two elder brothers who had always loved me and protected me. I also thank my sisters-in-law and other members of the greater family for their love, expectation, encouragement and praise.

Finally and most importantly, my deepest thank goes to Tingting for her love, support and accompaniment which made my study and my life so enjoyable.

And to my daughter Ruyan, for all the joys she has brought to our family!

# Contents

Abstract . . . . .	iii
Acknowledgements . . . . .	iv
List of Tables . . . . .	x
List of Figures . . . . .	xi
<b>1 Introduction</b>	<b>1</b>
1.1 Overview of Display Technologies . . . . .	1
1.1.1 Cathode-Ray Tube . . . . .	2
1.1.2 Liquid Crystal Display . . . . .	3
1.1.3 Plasma Display . . . . .	3
1.1.4 Organic Light-Emitting Diode Display . . . . .	4
1.1.5 Summary . . . . .	6
1.2 Full-Color Approaches . . . . .	7
1.2.1 Side-by-Side R, G, B Architecture . . . . .	8
1.2.2 White OLED with Color Filter . . . . .	9
1.2.3 Blue OLED with Color Changing Media . . . . .	11
1.2.4 Vertical Stack R, G, B Architecture . . . . .	11
1.3 Thesis Organization . . . . .	12
<b>2 Preview of Patterning Methods for Full-Color OLED Displays</b>	<b>14</b>
2.1 Ink-Jet Printing . . . . .	14
2.2 Dye Diffusion . . . . .	16

2.3	Laser-Assisted Patterning . . . . .	17
2.3.1	Laser-Induced Thermal Imaging . . . . .	17
2.3.2	Laser-Induced Sublimation . . . . .	18
2.4	Modified Photolithography . . . . .	20
2.4.1	Photosensitive Light-Emitting Polymer . . . . .	20
2.4.2	Dry Photolithography . . . . .	21
2.5	Relief Printing . . . . .	21
2.6	Patterning Methods for Small Molecule OLEDs . . . . .	22
2.6.1	Shadow-Mask-Assisted Thermal Evaporation . . . . .	22
2.6.2	Organic Vapor Jet Printing . . . . .	23
2.6.3	Molecular Jet Printing . . . . .	24
2.6.4	Small-Molecule Stamping . . . . .	25
2.7	Outlook . . . . .	26
<b>3</b>	<b>Device Fabrication</b>	<b>29</b>
3.1	Substrate and Anode . . . . .	29
3.2	Light Emitting Layer . . . . .	31
3.3	Cathode . . . . .	33
3.4	Device Test . . . . .	33
<b>4</b>	<b>Large-Area Wet Micro-Printing</b>	<b>40</b>
4.1	Concept of Large-Area Wet Micro-Printing . . . . .	41
4.2	Surface Energy Patterning of the Printing Plate . . . . .	41
4.2.1	Wettability . . . . .	42
4.2.2	Zisman Plot . . . . .	43
4.2.3	High Energy vs. Low Energy Surfaces . . . . .	45
4.2.4	Fluorinated Surface . . . . .	45
4.2.5	Printing Plate Fabrication . . . . .	48

4.3	Printing Apparatus . . . . .	50
4.4	Printing Experiments . . . . .	55
4.4.1	Printing Procedure . . . . .	55
4.4.2	Printing Solvents . . . . .	57
4.4.3	Printing Small Molecules . . . . .	57
4.4.4	Printing Polymers . . . . .	58
4.5	Device Performance and Solvent Revisited . . . . .	64
4.5.1	Modified Printing Setup . . . . .	66
4.5.2	Device Measurement . . . . .	68
4.5.3	Passive Matrix Display . . . . .	72
4.6	Summary . . . . .	75
<b>5</b>	<b>Profile Optimization for Wet-Printed Polymer Films</b>	<b>76</b>
5.1	Overview . . . . .	76
5.2	Profile Non-Uniformity . . . . .	77
5.3	Co-solvent Approach for a Uniform Profile . . . . .	78
5.4	Surfactant Approach for a Uniform Profile . . . . .	87
5.4.1	BASF Pluronic Surfactant . . . . .	88
5.4.2	3M Fluoro-Surfactant . . . . .	90
5.4.3	Unsolved Issues Related to Surfactant Approach . . . . .	95
5.4.4	Solvent Vapor Annealing . . . . .	97
5.5	Droplet Profile Study . . . . .	100
5.6	Summary . . . . .	118
<b>6</b>	<b>Transfer Printing</b>	<b>119</b>
6.1	Overview . . . . .	119
6.2	Concept of Transfer Printing . . . . .	119
6.3	Transfer Printing . . . . .	120

6.4	Transfer Printing PMMA . . . . .	127
6.5	Finite Element Analysis . . . . .	130
6.6	Transfer Printing Light-Emitting Polymer . . . . .	133
6.7	Critical Conditions for Successful Printing . . . . .	139
6.8	Fundamental Limiting Mechanism . . . . .	144
6.9	Device Characterization with Printed Polymer Films . . . . .	146
6.10	Summary . . . . .	151
<b>7</b>	<b>Transfer Printing Without Polymer Edge Breaking</b>	<b>153</b>
7.1	Overview . . . . .	153
7.2	The Hard-Hard Approach . . . . .	154
7.2.1	Concept of the Hard-Hard Approach . . . . .	154
7.2.2	Printing Results . . . . .	155
7.3	The Hard-Soft Approach . . . . .	160
7.3.1	Concept of Hard-Soft Approach . . . . .	162
7.3.2	Printing Results . . . . .	163
7.4	Summary . . . . .	170
<b>8</b>	<b>Conclusion</b>	<b>171</b>
8.1	Summary . . . . .	171
8.2	Future Work . . . . .	171
8.2.1	Transfer Printing Small Molecules . . . . .	171
8.2.2	Printing Color Filters . . . . .	172
	<b>Bibliography</b>	<b>174</b>

# List of Tables

3.1	Conversion factor $F_{conv}$ for different dye OLED [54] . . . . .	37
4.1	Surface tensions of commonly used liquids and substrates . . . . .	47
5.1	Key properties of several solvents at 25°C . . . . .	86
5.2	Comparison of surfactant on the effect of reducing surface tension of water . . . . .	91
6.1	Material parameters used in finite element analysis [10,43] . . . . .	132

# List of Figures

1.1	Products with an OLED screen in the market . . . . .	6
1.2	Four different approaches for achieving full-color OLED. (a-c) have a side-by-side R, G, B subpixel arrangement where in (a) R, G, B OLED subpixels are used, and in (b) white OLED in combination with color filters are used, and in (c) blue OLED in combination with color-changing media are used. Approach (d) uses a vertical R, G, B OLED subpixel arrangement [19]. . . . .	8
1.3	OLED micro-displays made by eMagin Corporation. (a) Micro-displays SVGA+ with 0.61" diagonal and $852(\times 3) \times 600$ pixels, (b) Micro-displays used in a head-mounted displays with 3D capability, (c) OLED structure utilized in the micro-display module. A white OLED combined with color filters are used in order to generate the R, G, B subpixels required in a full-color display. . . . .	10
2.1	Schematic diagram of the dye diffusion process [54]. . . . .	16
2.2	Laser-induced thermal imaging (LITI) method developed by 3M and Samsung [45, 47]. . . . .	18
2.3	Schematic diagram of the relief printing method [42]. . . . .	22
2.4	Schematic diagram of the organic vapor jet printing process [59]. . . . .	23
2.5	Illustration of the molecular jet printing apparatus and process [12]. (a) Shutter is open (b) Shutter is closed. . . . .	25

2.6	Schematic diagram of the small-molecule stamping process [13]. . . .	26
3.1	Structure of a standard OLED . . . . .	30
3.2	Chemical structures of various compounds used in this thesis. (a) PVK host polymer acting as hole transport layer, (b) PBD for electron transport, (c) green dye C6 (d) red dye nile red, (e) blue dye C47. . .	32
3.3	Electroluminescence spectra of standard PVK/PBD devices doped with C47, C6 or nile red [54]. . . . .	32
3.4	A photo of the testing setup, including the photodiode and a cable leading to the parameter analyzer, the microscope and micro-manipulators with probe tips. . . . .	35
3.5	Photodetector response spectra for PIN-10DP (DP series) from UDT Sensors, Inc. . . . .	36
3.6	Various OLED curves from a typical PVK:PBD:C6 OLED fabricated as described in Section 3.1-3.3. . . . .	38
3.6	Various OLED curves from a typical PVK:PBD:C6 OLED fabricated as described in Section 3.1-3.3. (cont'd) . . . . .	39
4.1	Schematic diagram of Large-Area wet Micro-Printing (LAMP) technique for organic device patterning. a) a surface-energy-patterned printing plate is coated with red “ink”; b) the printing plate is brought into contact with the device plate, i.e., to print; c) the printing plate is separated from the device plate and the transferred “ink” is allowed to dry; d,e) steps a-c are repeated for green and blue sub-pixels. . . .	42
4.2	A small droplet in equilibrium over a horizontal surface: (a) and (b) correspond to partial wetting, the trend towards wetting being stronger in (b) than in (a). (c) corresponds to complete wetting ( $\theta_e = 0$ ) [17]. .	43

4.3	A typical Zisman plot for a Teflon surface in contact with n-alkanes liquids (modified from [20]). The critical surface energy $\gamma_c$ for this system is about 18 mN/m. . . . .	44
4.4	Schematic diagram showing the chemical structure of PFOTS. . . . .	46
4.5	One possible structure of the PFOTS layer formed on a $\text{SiO}_x$ surface. . . . .	47
4.6	Procedures used for the fabrication of the printing plate. . . . .	49
4.7	Printing plates coated with various liquids by dip coating, showing the ability of selective wettability. . . . .	49
4.8	Printing plates coated with organic solution (a, c) then allowed to dry, which resulted in a thin organic layer pattern (b, d). . . . .	51
4.9	Lab setup used for the LAMP printing. . . . .	52
4.10	Schematics of laser alignment system. . . . .	53
4.11	Improved laser alignment system with interference stripe patterns shown. . . . .	55
4.12	An example of the fringe pattern formed on the aperture screen, taken when the alignment is close to best. The black square on the screen has a dimension of 10 mm $\times$ 10 mm. The center stripe has a spacing of about 5.4 mm, illustrated by the two arrows. The alignment accuracy is estimated to be about 12 arcseconds. . . . .	56
4.13	Solvent droplets printed onto glass substrates as demonstrations of the LAMP method. Droplets have a spacing of $600\mu\text{m}$ for both images. . . . .	57
4.14	Small molecular dye (C6) printed onto a glass substrate pre-coated with a PVK+PBD layer. Spacing between pixels are $600\mu\text{m}$ . . . . .	59
4.15	PVK+PBD+C6 in trichlorobenzene printed onto a glass substrate. . . . .	60

4.16	Printed green mixture with trichlorobenzene onto a $\text{SiN}_x$ patterned glass substrate. (a) Schematics of the printing, (b) UV photoluminescent image of the printed array, (c) an optical micrograph of a typical printed pixel, (d) a typical surface profile scan of the printed layer (dashed line is the outline of the well). . . . .	62
4.17	Printing onto a droplet constrained substrate. (a) Schematics, (b) UV photoluminescence of the printed arrays showing improved uniformity of pixel dimensions due to the confinement of droplets on the substrate. (c) A typical surface profile scan of the printed film (dashed line is the outline of the well). . . . .	63
4.18	Schematics for the printing of RGB arrays. . . . .	64
4.19	RGB arrays formed by three successive steps. . . . .	65
4.20	Effect of trichlorobenzene solvent on device I-V curves. Curves shown here are typical curves of device current and detected photocurrent vs applied voltage measured on devices containing the green-emitting mixture PVK+PBD+C6 deposited by various methods: (a) spin coating of green mixture in chlorobenzene solvent (control device), (b) spin coating of green-emitting mixture in trichlorobenzene, (c) green-emitting mixture in trichlorobenzene printed by LAMP method, (d) spin coat trichlorobenzene solvent followed by baking, then spin coating of green-emitting mixture in chlorobenzene solvent. . . . .	67

4.21	LAMP printing achieved with chlorobenzene solvent within a vapor saturated close system. (a) A plastic glove bag is used to form a closed system. Printing is done within the glove bag where the atmosphere has been saturated with chlorobenzene solvent vapor to extend the lifetime of droplets to allow enough time for printing. (b) Printing results of green pixels with chlorobenzene as solvent within the glove bag. . . . .	69
4.21	I-V curves of OLEDs with organic layer deposited by spin-coating (solid line) or printing (dash line) with chlorobenzene solvent. (a) OLED injection current (b) OLED photo current (c) Calculated external quantum efficiency. . . . .	71
4.22	A passive matrix display (by spin coating) under test. The printed circuit board is also shown. 6 rows $\times$ 12 columns of pixels are driven. The third row is missing, probably caused by a shorted pixel. . . . .	73
4.23	A passive matrix OLED display, with the light-emitting layer spin-coated, is driven with three different patterns. . . . .	74
4.24	A passive matrix OLED display with light-emitting layer printed by the LAMP method. (a) An optical micrograph (combined) showing 3 $\times$ 6 pixels after the printing of PVK+PBD+C6 layers. Vertical stripes shown are ITO anodes. Horizontal cathode stripes will be deposited later. (b) A 4 $\times$ 7 array under test. . . . .	74
5.1	Optical micrographs of the dried PVK films on flat substrate versus volume percent of dichlorobenzene in total solvent. Although coffee rings still exist in all six cases, the introduction of dichlorobenzene does change the profile for most of the pixel areas. In particular, the contrast of the deposited PVK film with 15% dichlorobenzene seems to have the best uniformity. . . . .	80

5.2	Profile scans of PVK films deposited on a flat substrate at various percentage of dichlorobenzene in chlorobenzene solvent, corresponding to Figure 5.1. The best profile is achieved with about 15% of dichlorobenzene. . . . .	81
5.3	3D profile of PVK film deposited with 15% dichlorobenzene in chlorobenzene solvent, corresponding to Figure 5.1b. The profile is quite uniform in the center, but the “coffee ring” is still present. . . . .	82
5.4	Typical profile of PVK film deposited into a well vs. the percentage of dichlorobenzene in chlorobenzene solvent. The first sub-figure shows the well-shaped substrate being used for all experiments. The best profile of the deposited film is achieved at about 15% of dichlorobenzene in chlorobenzene. . . . .	84
5.5	Typical profile of PVK film deposited into a well vs. the percentage of chloroform in chlorobenzene solvent. It is difficult to achieve a flat profile. . . . .	85
5.6	Profile of deposited PVK films (solid lines) versus L62 concentration in the solution. Three different substrates with well depth at 250 nm, 410 nm, 700 nm are used for the study and the profile of the wells are illustrated by dashed lines. PVK profiles are almost flat with 0.1 vol% of L62 added to the solution. . . . .	89
5.7	Device curves of OLEDs without surfactant (solid line) and with L62 surfactant at 0.05% (dashed line) added to the solution. PVK+PBD+C6 is used as the light-emitting layer. The addition of small amount of L62 surfactant caused significant degradation to the OLED device performance. . . . .	90

5.8	Profiles of deposited PVK films (solid lines) with the addition of FC-4432 surfactant. Four substrates with different well depth (illustrated with dashed lines) are used for the study. PVK profiles are almost flat with 0.0045 wt% of FC-4432 in the solution. . . . .	91
5.9	Effect of profile on electroluminescence uniformity. (a) Schematic of the device structure. (b) Typical profiles without surfactant and with FC-4432 at 0.0045 wt%. Dashed lines shows the well profile. (c) Electroluminescent micrograph of a 300 $\mu m$ -diameter pixel with PVK layer deposited without profile optimization. (d) Electroluminescent micrograph of a 300 $\mu m$ -diameter pixel with optimized PVK layer profile. White circles denote the pixel edges defined by the well opening. . . .	93
5.10	AFM surface area scan in overlay with the electroluminescent image. The two images have a great match of contrast with each other, which indicates that thick films of the light-emitting layers resulted in dimmed light emission. . . . .	94
5.11	Device curves of OLEDs without surfactant (solid line) and with the addition of FC-4432 surfactant at 0.0045 wt% (dashed line). PVK + PBD + C6 is used as the light-emitting layer. Only little changes on the curves are seen. . . . .	95
5.12	The profiles of PVK+PBD+C6 film vs the concentrations of L62 in the solution. The use of L62 does not flatten the profile of the mixture. . . . .	96
5.13	The effect of FC-4432 at 0.0045 wt% on the profiles of mixtures. A composition ratio of PVK:PBD:C6=100:40:0.3 is used. The well profile is given as dashed lines. . . . .	98
5.14	Effect of solvent vapor annealing on profiles. . . . .	99
5.15	Schematic diagram of the laser interferometer used to study the evolution of droplet profiles during evaporation. . . . .	101

5.16	Laser interferometer setup used for droplet profile study. . . . .	101
5.17	Five frames of the captured interference patterns from a trichlorobenzene droplet. Initial droplet diameter is $300 \mu m$ . . . . .	103
5.18	Line scan of the ring pattern shown in Figure 5.17c. The positions of peaks and valleys can be found. . . . .	104
5.19	Regenerated droplet profiles with spherical curve fitting of a trichlorobenzene droplet. . . . .	105
5.20	The droplet volume vs. time during solvent evaporation of a trichlorobenzene droplet. . . . .	105
5.21	Five frames of the captured interference patterns from a chlorobenzene droplet. Initial droplet diameter is $300 \mu m$ . . . . .	107
5.22	Regenerated droplet profiles with spherical curve fitting of a chlorobenzene droplet. . . . .	108
5.23	The droplet volume vs. time during solvent evaporation of a chlorobenzene droplet, and of a 0.1% PVK in chlorobenzene droplet. . . . .	108
5.24	Six frames of the captured interference patterns from a 0.1% PVK in chlorobenzene droplet. Initial droplet diameter is $300 \mu m$ . . . . .	109
5.25	Regenerated droplet profiles with spherical curve fitting of a 0.1% PVK in chlorobenzene droplet. The bottom curve deviates from a spherical shape so no fitting was applied and the absolute height of the droplet is unknown. . . . .	110
5.26	Six frames of the captured interference patterns from a 1% PVK in trichlorobenzene droplet. Droplet diameter is $300 \mu m$ . . . . .	111
5.27	Regenerated droplet profiles with spherical curve fitting of a 1% PVK in trichlorobenzene droplet. The bottom three curves have not been fitted and their absolute heights are unknown. . . . .	112

5.28	The droplet volume vs. time during solvent evaporation of a 1% PVK in trichlorobenzene droplet. . . . .	112
5.29	Four frames of the captured interference patterns from a 1% PVK in chlorobenzene droplet. Initial droplet diameter is 300 $\mu m$ . . . . .	113
5.30	Droplet shape evolution: 1% PVK in chlorobenzene. F1, F2, F4 and F6 are frame numbers. The droplet has a diameter of 300 $\mu m$ . Each curve is vertically offset from the next one by 1 $\mu m$ . . . . .	114
5.31	Four frames of the captured interference patterns from a 1% PVK in chlorobenzene droplet with 0.0045% FC-4432. Initial droplet diameter is 300 $\mu m$ . . . . .	115
5.32	Droplet shape evolution: 1% PVK in chlorobenzene with 0.0045% FC-4432. F2, F3, F4 and F7 are frame numbers. The droplet has a diameter of 300 $\mu m$ . Each curve is vertically offset from the next one by 1 $\mu m$ . . . . .	116
5.33	Top: Evolution of droplet profiles at different times during drying. Bottom: Side view of the drop with a typical “Mexican hat” shape. From Ref. [52]. . . . .	117
6.1	Basic patterning principle used in the transfer printing process. (a) Polymer film to be patterned is formed on top of a soft PDMS layer. (b) The hard stamp is pressed against the polymer film at elevated temperature to break the polymer film at protrusion edges. When the stamp is withdrawn, its raised features pick up the corresponding portions of the polymer layer. As a result, two patterned layers are formed, one on the stamp surface, another on the PDMS. (c) The polymer pattern on the stamp side in step (b) is transfer printed onto a target substrate. (d) The polymer pattern left on the PDMS side in step (b) is transfer printed onto a target substrate. . . . .	121

- 6.2 Schematic diagram of the transfer printing method for full-color OLED patterning. . . . . 122
- 6.3 Schematic diagram of the work-around used for alignment purposes. The alignment is done with a mask aligner with the transparent target substrate acting as the mask. When alignment is done, a small magnet is attached to the top of the stack which will hold the two wafers together. The whole stack is then transferred into the nano-imprinter for the actual transfer printing process. . . . . 127
- 6.4 PMMA patterns printed onto a silicon substrate after the second transfer step. The circular pads have a diameter of  $320\mu m$ , PMMA is shown in dark color and silicon is in light color. (a) PMMA film printed from the stamp surface. (b) PMMA film printed from the PDMS stamp side. 128
- 6.5 Surface profile scans of the two PMMA patterns shown in Figure 6.4, where positive pattern corresponds to Figure 6.4a and negative pattern corresponds to Figure 6.4b. . . . . 129
- 6.6 Typical results of “bad-quality” patterns as a result of partial transfer. PMMA is shown in dark color and silicon substrate is in light color. The partial transfer of the PMMA film is caused by a surface energy similarity between the silicon stamp (without any silane-treatment) and the silicon substrate. The circular pads have a diameter of  $320\mu m$ . 129
- 6.7 Various PMMA patterns formed by transfer printing. Three images in each row belong to a series where the first image is the pattern formed on the stamp (negative pattern) and the second image is the pattern formed on the PDMS layer (positive) and the third image is the second pattern transferred from PDMS onto a silicon wafer (positive). Different rows of images have different features (shape or dimension). 131

6.8	Finite element analysis results. (a) Model geometry, (b) Finite element mesh plot, (c) von Mises stress $\sigma$ distribution, (d) A magnification of (c) showing the region marked with the square, where large stresses are localized. . . . .	132
6.9	Transfer printing method utilized to pattern PVK + PBD + C6 green light-emitting layer. Optical micrographs of the polymer patterns at different steps are shown. (a) Rectangular-shaped areas are recessed silicon stamp surface and the rest is polymer on the unetched (raised) area (refer to Figure 6.2 label “I”). (b) Polymer rectangle ( $24\mu m \times 80\mu m$ ) array pattern left on the PDMS side (Figure 6.2 label “II”). (c) Polymer pattern shown in (b) is transferred onto a silicon target substrate by a second transfer step (Figure 6.2 label “III”). (d) Residue-free PDMS layer surface after the second transfer step (Figure 6.2 label “IV”). . . . .	134
6.10	Optical micrographs of transfer printed polymer patterns. (a) After the green and red-color subpixel arrays have been deposited. (b) After the RGB-subpixels have been deposited. . . . .	136
6.11	Two optical micrographs of transfer printed polymer patterns with R, G, B subpixels. Subpixel size is $24\mu m \times 80\mu m$ . . . . .	137
6.12	Surface profile scan of a typical transfer printed polymer film. The root-mean-square roughness is calculated to be $\sim 1.2$ nm from multiple scans. . . . .	138
6.13	Transfer printing method can pattern polymer layers with very sharp edges. Two micrographs of PVK+PBD+C6 patterns printed at $60^\circ C$ and 50 psi are shown at high magnification. Substrate is PDMS and size of the rectangles is $24\mu m \times 80\mu m$ . . . . .	140

6.14	Polymer layer pattern deposited by laser-induced thermal imaging (LITI) method [45, 47]. . . . .	141
6.14	Various polymer layer patterns (PVK+PBD+C6 on PDMS side) resulting from transfer printing experiments with different printing temperature and pressure settings (a)-(h). Minimum temperature and pressure required for a good-quality pattern can be inferred from these experiments and are plotted in (i). . . . .	143
6.15	The shear yield stress vs. $T-T_g$ for PC, PVC and PMMA. Data points taken from Ref. [41]. . . . .	146
6.16	The compression yield stress vs. temperature predicted by Ree-Eyring model for (a) PMMA and (b) PC. The Argon model is also shown for PMMA. Parameters used for the calculation are from Ref. [56] . . . .	147
6.17	Comparison of I-V characteristics of OLEDs with polymer film deposited by transfer printing ( $50^\circ C$ and 50 psi) and spin coating. . . .	148
6.18	Effect of printing temperature and pressure on OLED device performance. The external quantum efficiency is calculated for comparison. Efficiencies are compared to spin-coated control devices, which mostly fall into the range marked with the two dashed lines. Devices labeled with “spin + heat cycle” were prepared with spin-coating that had undergone the same thermal cycle with printed devices. . . . .	149
6.19	Effect of pressure on film thickness of the printed PVK+PBD+C6 layer.	151
7.1	Schematic diagram of the hard-hard approach of the transfer printing method. . . . .	155

7.2	The polymer layer formed by spin-coating on the stamp protrusion is non-uniform in thickness. (a) An optical micrograph of the polymer-coated stamp surface. (b) A typical surface profile scan of the polymer-coated stamp along the line shown in (a). The dashed line refers to the stamp substrate . . . . .	156
7.3	Printing results of the hard-hard approach at pressure 500 psi and at different temperature. Micrographs shown here are the final pattern of PVK+PBD+C6 blend after being transferred onto a silicon substrate.	158
7.4	Micrographs of the stamp surface after the transfer printing step. Incomplete vs. complete transfer are observed under different printing conditions. . . . .	159
7.5	Schematic diagram of the hard-hard approach in dealing with non-flat surface. . . . .	160
7.5	Optical micrographs of transfer printed polymer patterns. (a) After the printing of the green subpixel arrays. (b) After the printing of the red subpixel arrays. (c) After the green, red, and blue-subpixels have been deposited. . . . .	162
7.6	Schematic diagram of the hard-soft transfer printing approach. . . . .	163
7.7	Micrographs of the PDMS surface after the first transfer printing step. (a) No oxygen plasma treatment is performed on the PDMS surface before the transfer printing. No polymer is transferred onto the PDMS side (the contrast seen on the image is impression caused by the pressing of the hard stamp). (b) The PDMS is treated with an oxygen plasma for 30 seconds, which results in the successful transfer of the polymer films onto the PDMS. . . . .	164

7.8	Micrographs of the PDMS surface after the second transfer printing step. (a) With a short oxygen plasma treatment, the polymer pattern can be successfully transferred and no polymer film is left on the PDMS surface. (b) If the oxygen plasma treatment is too long, it is difficult to achieve a complete transfer of the polymer films in the second transfer step. . . . .	165
7.9	Polymer patterns at different stages of the hard-soft transfer printing approach. . . . .	166
7.10	Polymer patterns formed on the PDMS surface after the first soft-printing step. Printing temperature is $110^{\circ}\text{C}$ while pressure varies. . .	167
7.11	Schematic diagram of the hard-soft approach in dealing with non-flat surface. . . . .	168
7.11	Optical micrographs of transfer printed polymer patterns. (a) After the printing of the green subpixel arrays. (b) After the printing of the green and red subpixel arrays. (c) After the green, red, and blue-subpixels have been deposited. . . . .	170
8.1	An array of $\text{Alq}_3$ film printed onto an ITO-glass substrate, with features at $4\mu\text{m} \times 12\mu\text{m}$ . . . . .	172

## Introduction

### 1.1 Overview of Display Technologies

The electronic display is an important human/machine interface, because most information is presented in visual form. Far less information is presented in audio form. Electronic information display is nowadays a \$100 billion per year business and is expected to grow to \$140 billion by 2015 [70]. For 2007, television (TV) sets and other large-area applications make up 41% of the total display market, desktop and notebook monitors make up 35%, and the rest of the market is small/medium displays. Various display technologies exist, with mainstream technologies being cathode-ray tube (CRT), liquid crystal display (LCD), plasma display, etc. When comparing different display technologies, the main characteristics of a display that are of importance are [49]:

- Contrast ratio
- Brightness (luminance)
- Speed or response
- Resolution (dots/inch)
- Color depth and gamut

- Manufacturing cost
- Lifetime
- Power consumption
- Weight
- Volume
- Viewability (view angle, outdoor readability)

### 1.1.1 Cathode-Ray Tube

The first practical electronic information display technology was the CRT. Monochrome CRT TV was commercialized in the mid-40s with its large-scale production. Color CRT TV was shortly achieved afterwards with a shadow mask approach at RCA by its research lab (now Sarnoff Inc.) in Princeton, NJ. The success of the CRT as a display has been truly exceptional, despite the limitations of technologies available at that time. It has performed well in many of the characteristics listed above, namely contrast ratio, brightness, speed, resolution, color, cost, lifetime, etc. Since its inception and until very recently the CRT has been the single dominant display technology. The main disadvantages of the CRT come from the vacuum-tube and its 3-dimensional nature, so that CRT units are bulky, heavy and fragile. Tremendous amount of effort has been spent on the pursuit of an ideal light-weight flat-panel display. However, due to the success of CRT in many aspects as a display, the pursuit has been challenging and the ideal display has yet to be invented. Major players in the flat-panel display race includes liquid crystal displays, plasma displays and the emerging technology: organic light-emitting diode displays (OLED display). According to DisplaySearch [70], the LCD dominates the flat-panel display market with a

share of three quarters, with plasma displays at  $\sim 10\%$  in second and OLED displays at merely 1%.

### 1.1.2 Liquid Crystal Display

Similar to the invention of the color CRT, the liquid crystal display was invented at RCA by its research lab in Princeton, NJ [27]. The liquid crystal cell is used as a light valve, and thus the LCD is a non-emissive display. In its early stages, the LCD faced many technical challenges posed by the CRT standard, which included low contrast ratio, low response, short lifetime, high power consumption, etc. Thanks to many technical advances made on the LCD it is now the overwhelming choice in laptop notebook monitors, where the requirement of portability prohibits the use of CRTs. LCDs, due to their light-weight and flat-panel form, have also replaced the major CRT applications of desktop monitors and televisions. For 2007, the CRT revenue in desktop monitor was \$545 million. In contrast, the LCD desktop monitor had a revenue of \$25 billion, plus another \$12 billion in notebook monitors [70].

Despite its success, the transmissive LCD architecture still requires a backlight, polarizer, color-filter and liquid crystal cell acting as a light valve. The LCD structure and its non-emissive nature limits the power efficiency, response time and viewing angle, etc. A search for a display with a simpler approach is still worthwhile.

### 1.1.3 Plasma Display

The plasma flat panel display is another major player in the current display market and a main competitor to the LCD. The plasma display is self-emissive and it possesses many advantages of the CRT. It has excellent color and good viewing angle. Similar to the LCD, plasma displays are thin and light-weight in contrast to CRTs. Plasma displays tend to have relatively larger pixels, so the resolution is low compared to the LCD, and manufacturing cost is high. Plasma displays are believed to be able

to compete with LCDs only in displays of 30-70 inch diagonal where the LCD cost is also high. Luminance efficiency and lifetime are the two main issues related to plasma displays. With the intrusion of the LCDs into the large display market, the competition between plasma displays and LCDs is still intense.

### 1.1.4 Organic Light-Emitting Diode Display

Electroluminescence in organic materials was first reported by Pope in 1963 [53]. Light emission was observed from single crystals of anthracene when a high voltage was applied. In 1987 Tang and Van Slyke [61,62] of Eastman Kodak pioneered the first multi-layer structure and obtained high efficiencies and low voltage in small molecule films. Light emission from conjugated polymers was also reported later [9]. A simple OLED structure contains an anode layer, which is usually transparent indium-tin oxide (ITO), one or more organic layers and a cathode layer.

Compared with the LCD technology, the OLED display may have advantages in many aspects, as itemized in the following list.

- Thin and light-weight
- Broad color gamut
- High contrast
- Fast response
- Large viewing angle
- Low power consumption
- Potentially non-fragile and flexible
- Low structure complexity
- Potentially low cost

The OLED is self emissive so that a backlight is not necessary and the power consumption is low. In addition, the emission from an OLED pixel has been previously measured to be very close to Lambertian emission [61], so the OLED display will have very wide angles.<sup>1</sup> Next, the OLED can be made even thinner and more light-weight compared to LCD displays. The OLED has a faster response than LCD, which is good for video applications. Organic materials can be deposited onto various substrates and thus can be made non-fragile or even flexible. Thanks to the abundance of organic materials, OLED offers a wide color gamut, far superior compared to any other display technology to date.

After two decades of research and development, OLEDs have been used in many products, ranging from mobile phones, portable digital audio players (MP3 players), car radios, digital cameras, camcorders, head-mounted displays to television sets. In early 2003 Kodak introduced the world's first digital camera with an OLED screen (Kodak EasyShare LS633, Figure 1.1a). In late 2007 Sony commercialized the world's first OLED TV, with an 11" screen (Sony XEL-1, Figure 1.1b). Specifications of the Sony OLED TV clearly demonstrated several of the advantages we have listed above for OLED displays. For example, it is only 3 mm thick and 1.9 Kg in weight with the stand. The dynamic contrast is over 1,000,000:1 and the viewing angle is 178 degrees. The OLED TV has a color reproduction greater than 100% NTSC color gamut (CRTs and LCDs both have a limit at about 70-75% NTSC). A 27-inch OLED TV from Sony

---

<sup>1</sup>Lambert's Law of Emission, also known as Lambert's Cosine Law, states that for an ideal diffuse radiating surface the intensity emitted in any direction is proportional to the cosine of the angle between the normal to the surface and the radiation direction (or viewing direction).

$$I(\theta) = I_0 \cos(\theta) \quad (1.1)$$

For a small portion of the radiating surface with an area of  $A$  viewed at an angle  $\theta$ , since the projected area is also proportional to the cosine of the angle, the luminance (luminous intensity per unit area) is then:

$$\frac{I_0 \cos(\theta)}{A \cos(\theta)} = \frac{I_0}{A} \quad (1.2)$$

which is independent of the viewing angle. In other words, the radiating surface appears equally bright regardless of the viewing angle.



(a) Kodak EasyShare LS633 digital camera



(b) Sony XEL-1 OLED TV

Figure 1.1: Products with an OLED screen in the market

will be soon on the market. For a near-complete list of current OLED products, see Ref. [1].

### 1.1.5 Summary

OLED displays are not yet able to displace LCDs from the market despite their potential. One issue is related to the material stability and the OLED device lifetime. Another issue of the OLED is its manufacturing cost. For example, Sony's 11" OLED TV now sells at \$2500. One reason of the high manufacturing cost is that non-conventional patterning techniques are required in order to achieve full-color OLED displays. The goal of this thesis work is to develop new low-cost methods for OLED patterning so that the manufacturing cost of OLED displays can be competitive or even lower than LCD displays.

The CRT, LCD, plasma and OLED displays discussed so far all belong to the category of volatile displays. In contrast, a static display is a display that requires no energy to maintain its information, rather it only requires energy to change the information. Examples of static displays includes electrophoretic displays (E Ink Inc.),

cholesteric liquid-crystal displays (Kent Display), MEMS-based displays (Qualcomm's iMod), etc. Static displays are good for some niche markets where a very low power consumption is required while a slow refresh rate is acceptable and are not the focus of this thesis.

## 1.2 Full-Color Approaches

In a color display, a pixel is usually formed with closely spaced subpixels each emitting one of the primary colors of red, green and blue (R, G, B). By the relative brightness emitted by each of the three subpixels, different colors are perceived by human eyes, which will automatically merge the subpixels into one pixel at some distance. In a CRT display, R, G and B subpixels are formed by an electron beam hitting different phosphorescent layers. In an LCD display, a white fluorescent backlight is used and color filters are used in order to form R, G and B subpixels. For an OLED display several approaches can be exploited to generate full-color ability [19], as shown in Figure 1.2. Since an OLED can emit light in different colors by changing the light-emitting organic layer, the simplest way is to use R, G and B OLED subpixels side-by-side, as shown in Figure 1.2a. Another scheme is to use color filters similar to the one adopted by LCD displays as shown in Figure 1.2b. In this scheme, a white OLED is used and by using three different color filters, R, G, B subpixels can be formed. In a similar scheme as shown in Figure 1.2c, a blue OLED is used rather than a white OLED. Color-changing media are used for down-converting blue light into green or red emission to form G, R subpixels. The previous three approaches all use a side-by-side R, G, B arrangement, but in an alternative way they could also be stacked vertically to form a pixel. As shown in Figure 1.2d, a pixel can be formed by fabricate R, G, B OLED subpixels on-top-of each other, provided that each subpixel is still individually addressable and transparency through the multi-layers stack is

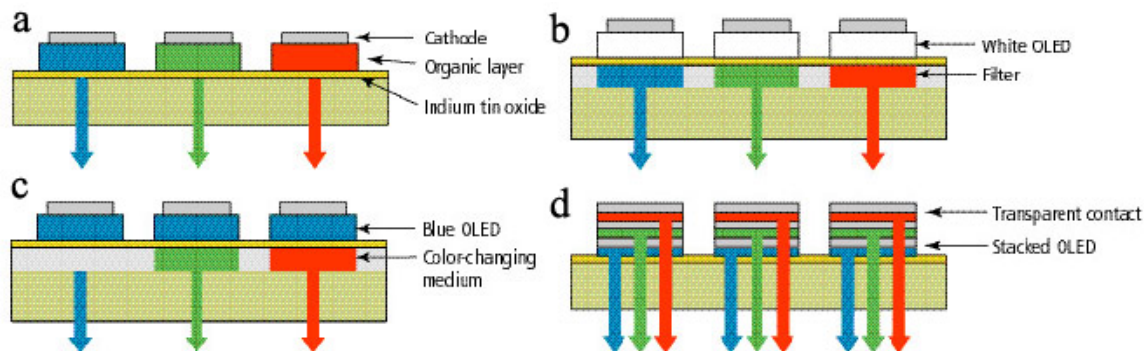


Figure 1.2: Four different approaches for achieving full-color OLED. (a-c) have a side-by-side R, G, B subpixel arrangement where in (a) R, G, B OLED subpixels are used, and in (b) white OLED in combination with color filters are used, and in (c) blue OLED in combination with color-changing media are used. Approach (d) uses a vertical R, G, B OLED subpixel arrangement [19].

retained.

### 1.2.1 Side-by-Side R, G, B Architecture

In the scheme of a side-by-side R, G, B subpixel configuration (Figure 1.2a), three closely spaced color segments are required which will emit light in either R, G or B color. Thus a method able to deposit three different light emitting layers side-by-side is required. Conventional photolithography is usually not suitable for organic layer patterning, since the solvent process will degrade the organic materials, and because of the cost. Hence, novel patterning techniques are desired in order to fabricate the R, G, B subpixel OLED. Compared with the other three schemes, the use of side-by-side R, G, B emitters has the advantage of high power efficiency, and it takes advantage of the abundant kinds of light-emitting organic materials available so that a wide color gamut can be achieved for the final display. At the same time, differential aging of the R, G, B subpixels need to be compensated for.

As an example, the display of Eastman Kodak's EasyShare LS633 digital camera shown in Figure 1.1a has a side-by-side R, G, B architecture design. Sony's 11" OLED TV (Figure 1.1b) is also based on this R, G, B subpixel arrangement (color filters are

also used to achieve a broader color gamut).

### 1.2.2 White OLED with Color Filter

In the scheme of white OLEDs with color filters (Figure 1.2b), only a white OLED is required, so a patterning method for the OLED emissive layer is not necessary. On the other hand, it does require a patterning technique to deposit the three color filters used to form the R, G, B light emission subpixels. The color filters, however, are also used in the LCD display manufacturing, and they can be patterned by the photolithographic method, which can be easily adopted to OLED manufacturing. Since a uniform white OLED is used, differential aging is not a big issue for the color. One disadvantage of this scheme is that the device power efficiency is low due to the loss of large amount of light through the color filters. In addition, a special OLED which will give out white light emission is also required. Further, the color gamut is controlled by the spectrum of the white OLED. Eastman Kodak utilized this white OLED with color filter scheme in their 15" prototype jointly developed with Sanyo.

eMagin Corporation has several OLED micro-display OEM modules on the market (Figure 1.3). The OLED structure used in their micro-displays is shown in Figure 1.3c. White OLEDs combined with color filters are used, licensed from and based on Kodak's technology.

In order to improve the efficiency of this approach, Kodak further developed an modified white OLED-color filter architecture. In this architecture, a white subpixel (generated from the white OLED without color filter) is also added in addition to the R, G, B subpixels. Due to the presence of the white subpixel, the fact that it does not undergo the absorption of color filters, and the fact that a large portion of a regular image contains white, the display efficiency is greatly improved.

Another way to generate R, G, B color from a white OLED is to use the microcavity effect [40]. However, the color and luminance generated by the microcavity effect

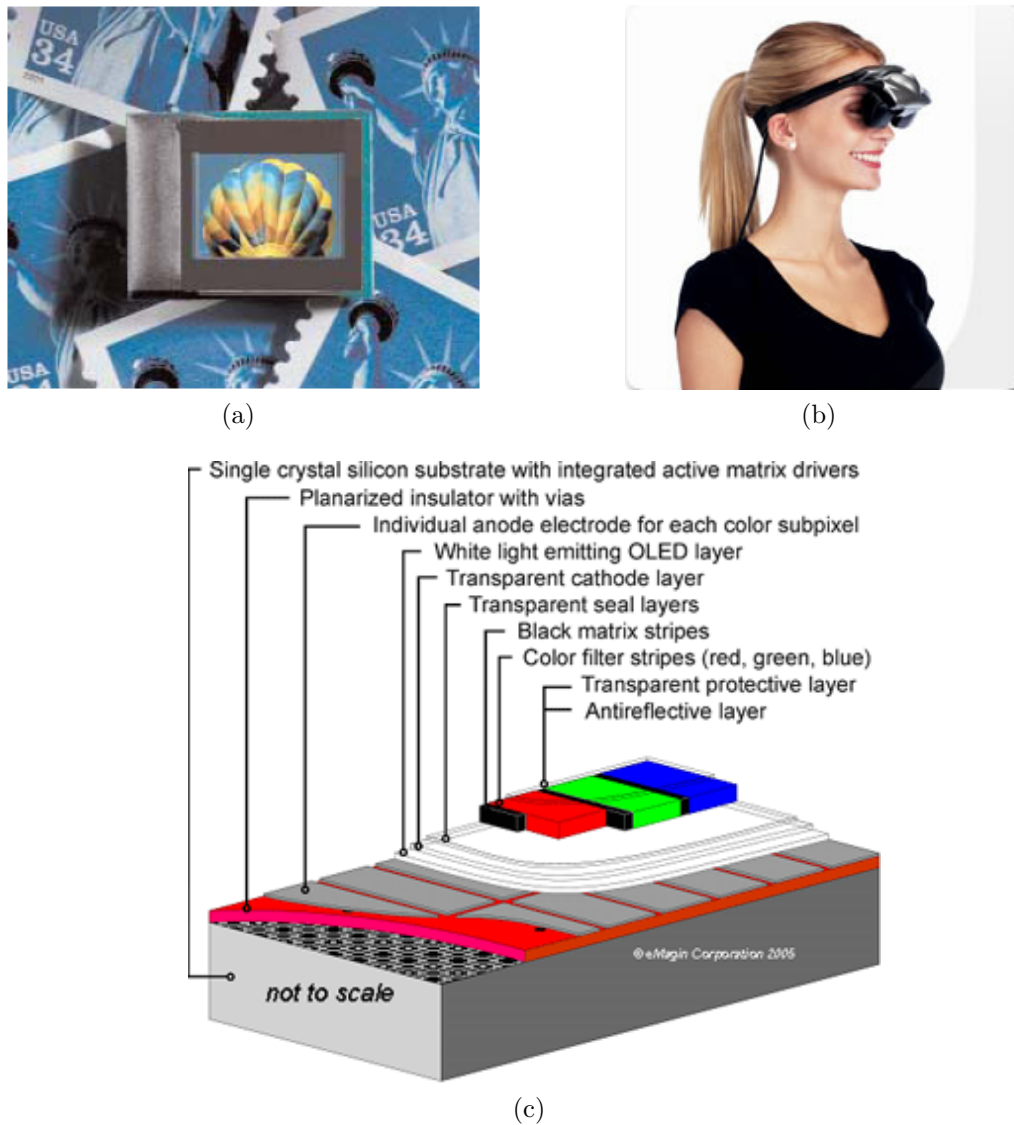


Figure 1.3: OLED micro-displays made by eMagin Corporation. (a) Micro-displays SVGA+ with 0.61" diagonal and  $852(\times 3) \times 600$  pixels, (b) Micro-displays used in a head-mounted displays with 3D capability, (c) OLED structure utilized in the micro-display module. A white OLED combined with color filters are used in order to generate the R, G, B subpixels required in a full-color display.

depend on the viewing angle, which is a concern for display applications. In fact, a white OLED with microcavity plus color filter structure has also been demonstrated, which outperforms in color gamut and brightness of the white OLED with color filter configuration, and reduces the viewing angle dependence observed in white OLED with microcavity configuration [40].

### 1.2.3 Blue OLED with Color Changing Media

The use of blue OLEDs with color changing media (Figure 1.2c) is to some extent similar to the scheme with white OLEDs combined with color filters (Figure 1.2b) but may have higher power efficiency. Instead of a white OLED, it uses a blue OLED. Color-changing media (also called organic fluorescent wavelength down-converters) are used, which efficiently absorb the blue light and re-emit green or red light. As shown in Figure 1.2b, a blanket blue OLED layer is used, which does not require any patterning. In this scheme, the display power efficiency is higher than that of a white OLED with color filters since the blue light does not undergo any filtering, and the loss due to down-conversion (for green and red subpixels) may be less than that in a color filter. Compared to the R,G,B emitter scheme shown on Figure 1.2a, it also suffers from low power efficiency, however.

### 1.2.4 Vertical Stack R, G, B Architecture

Shen et al. demonstrated a vertical R, G, B OLED pixel in 1997 [57]. Compared with side-by-side pixel architectures (Figure 1.2 a,b,c), this vertically-stacked pixel arrangement offers larger areas for each R, G, B subpixel for the same total pixel size. Thus pixels can be driven with significantly lower voltage in order to achieve the same luminance. In addition, it is not necessary to laterally pattern the different layers used for R, G, B subpixels.

The vertical R, G, B architecture has many disadvantages, however. First, the

multi-layer structure is very complex in manufacturing. For example, in Shen's paper [57] a 12-layer device structure and a six-mask process is utilized. Second, since the R, G, B subpixels are electrically connected with each other, the driving circuit is also complex in order to address each subpixel separately. Third, the light output is low due to multi-layer absorption, especially since several cathode layers (usually metal) are present. In addition, the light emission spectra from each subpixel in the vertically stacked structure differ substantially from their discrete devices, mainly due to an energy down-conversion process and the microcavity effect [57]. This spectra variation will further complicate the practical display design. Based on these disadvantages, the vertically stacked RGB architecture will take more time to crossover from development to production.

In summary, since the schemes shown on Figure 1.2b and Figure 1.2c have a low power efficiency and Figure 1.2d is excessively-complex in design and manufacturing, the scheme shown on Figure 1.2a (direct patterning of R,G,B emitters) is the preferred choice, provided that a low-cost patterning method is available for the organic layer patterning. The development of novel patterning methods for organic layer patterning is exactly the goal of this thesis.

### 1.3 Thesis Organization

This thesis focuses on developing novel patterning techniques for depositing polymer layers to form the RGB subpixels for a full-color display. In Chapter 2 an overview of different patterning techniques that have been developed is given. In Chapter 3 the material system, device structure, general fabrication and testing procedures, etc., are discussed. In Chapter 4 we present a wet printing method: Large-Area Wet Micro-Printing (LAMP). Since wet-printed polymer films have a non-uniform thickness, in Chapter 5, two approaches are utilized in order to achieve a flat profile

for wet printed films. In Chapter 6 we introduce a transfer printing method to deposit polymer films, which has very high resolution and very uniform films. In Chapter 7 another transfer printing method is introduced, where polymer films to be patterned are directly deposited on a stamp surface. Finally, Chapter 8 is a brief summary of the thesis and a discussion of some future research directions.

# Preview of Patterning Methods for Full-Color OLED Displays

As discussed in Chapter 1 Section 1.2, for a full-color OLED display a side-by-side subpixels arrangement, which emits in R, G, B color is preferred due to its high power efficiency and low complexity. Organic layers for small molecule OLEDs are deposited by evaporation. Polymer films can be deposited by a simple spin-coating process. However, the as-deposited films (either by evaporation or by spin-coating) are homogeneous and are only good for monochrome displays. In addition, patterning and etching of active organic layers is difficult with photolithography and wet etching, due to their sensitivity to solvents. Soon after the discovery of high-efficiency organic light-emitting devices by Tang [61], research on new patterning methods able to deposit and pattern light emitting organic materials became one of the main fields within the OLED community. In this chapter, an overview is given on several patterning techniques that have been explored.

## 2.1 Ink-Jet Printing

Ink-jet printing of polymers is one of the alternatives investigated to selectively deposit R, G, and B pixels side-by-side. Pioneering work of using ink-jet printing for OLED

patterning was done in our lab [26]. There have been many following works on ink-jet printing by OLED display manufacturers such as Seiko-Epson Corp [58], Cambridge Display Technology [4,11] and Samsung [44]. Seiko-Epson demonstrated a 40" OLED TV with its R, G and B pixels deposited by ink-jet printing.

Advantages of ink-jet printing include:

- Ink-jet printing is a digital process which does not require a mask. It is easily adaptable to different designs, thus reducing tooling cost.
- It is an additive process and has high use efficiency of materials. This also means greatly reduced processing steps since sacrificial layers (such as photoresist) and further etching or removing step are not required.
- It is a non-contact process so contact contamination is not an issue.
- It is easy to handle large substrates.

Limitations or disadvantages of ink-jet printing include:

- Ink-jet printing (without special step) has a low resolution. A typical resolution of 60  $\mu m$  is reported.
- It has a low throughput since printing is a serial process.
- The printed film thickness is usually uneven, which will result in non-uniform light emission. In order to achieve the desired film shape, thickness and properties, it is necessary to properly control the ink formulation, the surface energy of the substrate and the vaporization process of the solvent.
- The droplet position accuracy and droplet volume consistency are low. Usually, the substrate morphology (such as a well for droplet confinement) and its surface energy pattern need to be properly prepared.

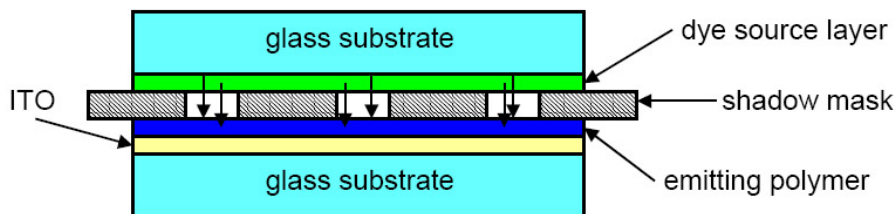


Figure 2.1: Schematic diagram of the dye diffusion process [54].

- There are some maintenance issues related to ink-jet printing, such as nozzle clogging.
- It is difficult to ink-jet print small molecules due to low viscosity.

## 2.2 Dye Diffusion

A dye diffusion method has been introduced in our group [54, 55]. The idea of introducing a small amount of dye into a previously-deposited uniform polymer layer is the basis for the dye transfer method. The dye is locally transferred over a large area into the polymer film and thus changes the emission color of the device. During the diffusion process, the dye desorbs from a donor film and diffuses into the polymer film through a mask layer. Figure 2.1 is a schematic diagram of the dye diffusion process. The diffusion may be assisted by solvent vapor to temporarily lower the glass transition temperature of the polymer layer [23]. For full-color patterning, this process can be repeated with different masks and dyes to create different color emitting regions. However, it may be difficult to keep the diffused dyes from bleeding into regions nearby.

## 2.3 Laser-Assisted Patterning

There have been several similar patterning methods developed so far that utilize a laser scanning exposure system. They are discussed in this section.

### 2.3.1 Laser-Induced Thermal Imaging

3M and Samsung introduced a laser-related patterning method called Laser-Induced Thermal Imaging (LITI) [45–47, 69]. In this method, a donor film with pre-deposited OLED materials is prepared by conventional methods such as spin-coating, web-coating or vacuum deposition (shown in Figure 2.2a). During the laser exposure process, the light-to-heat conversion layer of the donor film absorbs laser energy and expands in volume, which releases the OLED materials layer, which re-deposits onto a device substrate. Figure 2.2b shows several laser transferred patterns. The left image is laser transferred light-emitting polymer (LEP) stripes with a width of 80  $\mu\text{m}$ . A small molecule (SM) pattern is shown in the right and a 1:3 mixture of LEP and SM pattern is given in the middle.

Advantages of the laser-induced thermal imaging method include:

- It is a non-mask, digital process, which means it can easily adapt to new designs with minimum retooling cost.
- It can handle large substrates. Samsung is developing the laser thermal imaging process on a Gen 4 system.
- It has a relatively high resolution.
- Due to its dry transfer feature, the film thickness is uniform.
- It is possible to transfer a multi-layer stack at one time.
- It can handle small molecules quite well. Transferred small molecules have good pattern quality (right image of Figure 2.2b).

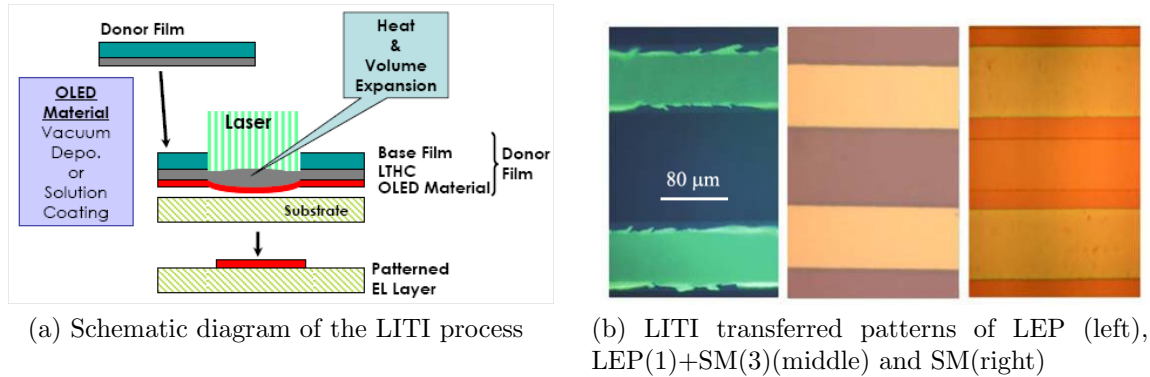


Figure 2.2: Laser-induced thermal imaging (LITI) method developed by 3M and Samsung [45, 47].

Disadvantages include:

- It is difficult to pattern polymer films [45, 46]. Due to the high strength of the polymer film, it is difficult to form a clean edge along the border between the imaged and unimaged regions (Figure 2.2b, left image is a  $80\mu\text{m}$ -wide polymer strip patterned by laser-induced thermal imaging).
- Contact between the donor film and the emitting area may degrade the device.
- The transferred layer interface is formed by a lamination process so there is a concern that the interface may affect the device performance or lifetime.
- Because the method is a contact printing technique, any particle contamination will prevent successful transfer of regions that are much larger than the particle size.

Samsung has demonstrated a 17" UXGA OLED display with laser-induced thermal imaging [47].

### 2.3.2 Laser-Induced Sublimation

Eastman Kodak introduced radiation-induced sublimation transfer (RIST) [6]. Sony developed a very similar method called laser-induced pattern-wise sublimation (LIPS)

[28]. These two methods both utilize a laser to sublimate small-molecule films pre-deposited on a donor film and re-deposit them onto a device substrate. Due to the similarity of these two methods, they will be referred to as laser-induced sublimation in this thesis for convenience. In Kodak's process, a polyimide plastic film is used as the substrate for the donor film while in Sony's case it is replaced by a glass substrate. The polyimide donor film might cause out-gassing problems during laser heating and a high precision technique is required to set the flexible donor film uniformly onto a large-scale glass substrate.

The laser-induced sublimation method is similar to the laser-induced thermal imaging method introduced earlier in that both a donor film and a laser scanning system are used. The difference lies in the mechanism of the release and re-deposition processes of the organic materials. In the laser thermal imaging method, it is basically a release/adhesion process which is caused by the volume expansion of the light-to-heat conversion layer. In the laser-induced sublimation method, however, an absorption layer (molybdenum or chromium) converts the laser energy to heat and the organic materials on the donor film are vacuum-sublimated and re-deposit on the device substrate.

Advantages of the laser-induced sublimation method include:

- It is a non-mask, digital patterning technique.
- It is a non-contact process so contamination or degradation due to contact is prevented.
- It can handle large substrates.
- The film thickness is believed to be uniform.
- The layer interface is formed in a way similar to thermal evaporation so the interface quality might not be an issue.

Disadvantages include:

- Since it is a vacuum sublimation process, it is limited to small molecules.
- In contrast to multi-layer capability of laser-induced thermal imaging, this method is only able to deposit a single layer at a time.

Sony has demonstrated a 27.3" OLED TV prototype with the laser-induced sublimation method [28]. The red and green emitting layers are patterned with laser-induced sublimation while the blue emitting layer is deposited as a common layer in the prototype.

## 2.4 Modified Photolithography

Conventional photolithography is not compatible with organic patterning since the solvent process will degrade the active light-emitting materials to be deposited. There has been some effort to develop a modified photolithography process that is compatible with active organic layer patterning. One approach used is to make the light-emitting polymer photosensitive such that the organic layer itself can be cross-linked by exposure to ultraviolet light and become non-soluble. Another approach is to develop a new photolithography procedure that is compatible with active organic layers.

### 2.4.1 Photosensitive Light-Emitting Polymer

In conventional photolithography, a photoresist layer is used as an etch mask for further patterning of the underlying layer. By rendering the light-emitting polymer to be photosensitive, it can be directly patterned by ultraviolet exposure, thus removing the use of photoresist. After exposure to ultraviolet light, the light emitting polymer becomes cross-linked and insoluble [21, 51]. This method can achieve relatively high

resolution. However, this method requires the synthesis of specialized photosensitive light-emitting polymers. Usually, these photosensitive light-emitting polymers will have compromised electrical or optical properties. Even so, the availability of such polymers is very limited which means it can not take advantage of the best performance (efficiency, color, life-time, etc) materials available.

### 2.4.2 Dry Photolithography

Another approach used to solve the compatibility issue is to use a new photoresist and solvent system which is compatible with most organic materials. One of this approach is demonstrated by a Cornell group and is called Dry Photolithography [29]. The main point of the dry photolithography is utilizing a super-critical carbon dioxide ( $\text{scCO}_2$ ) as the solvent for photoresist processing.  $\text{scCO}_2$  is a poor solvent for most organic compounds so it can be used as a non-destructive development medium. This dry photolithography method is compatible with the majority of organic materials. However, the organic layers for different colors still need to be spin-coated, and the solvent used should not dissolve the underlying layers that were deposited by the previous steps. On the other hand, photolithography for R, G, B patterning requires many more processing steps than other direct methods (ink-jet, etc), which is a concern from the cost perspective.

## 2.5 Relief Printing

The process of relief printing is given in Figure 2.3 [42]. A relief plate is attached to the cylinder roll which will pick up inks from the ink pan through the anilox roll (Figure 2.3a) and then transfer to device substrate by another step (Figure 2.3b). This method will have good use efficiency of light emitting polymers, and may have high resolution and high throughput. Since it is also a wet printing technique, the ink

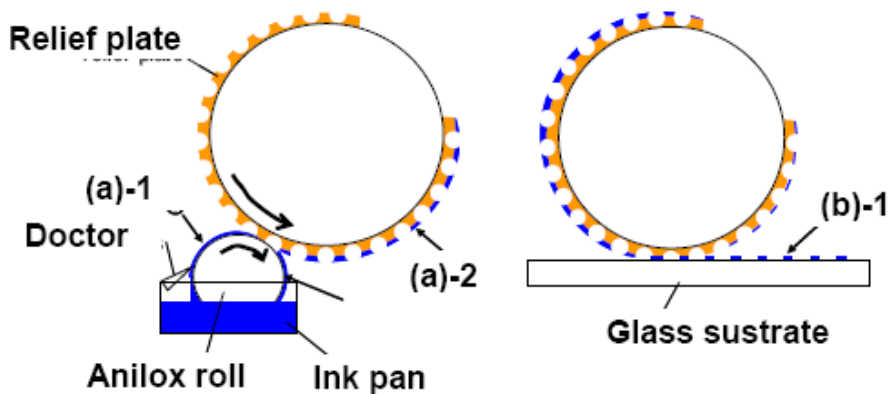


Figure 2.3: Schematic diagram of the relief printing method [42].

formulation needs to be tuned carefully in order to achieve a uniform film thickness.

## 2.6 Patterning Methods for Small Molecule OLEDs

Most patterning methods discussed so far are focused on the patterning of polymer films (except the laser sublimation). The following section introduces several other patterning techniques that are focused on the patterning of small molecules.

### 2.6.1 Shadow-Mask-Assisted Thermal Evaporation

Small molecules are usually deposited by thermal evaporation. For R, G, B color patterning a shadow mask is usually used. We refer to this method as shadow-mask-assisted thermal evaporation. Holes in the shadow mask are used to guide the deposition of small molecules; three successive vacuum deposition steps are required for R, G, B patterning. Multi-layer registration is also required. As an example, the Kokak Easyshare LS633 digital camera (Figure 1.1a) has a 2.2" OLED screen and shadow-mask-assisted thermal evaporation was used for the patterning.

Some concerns related to this method are:

- This method is only good for small molecules.

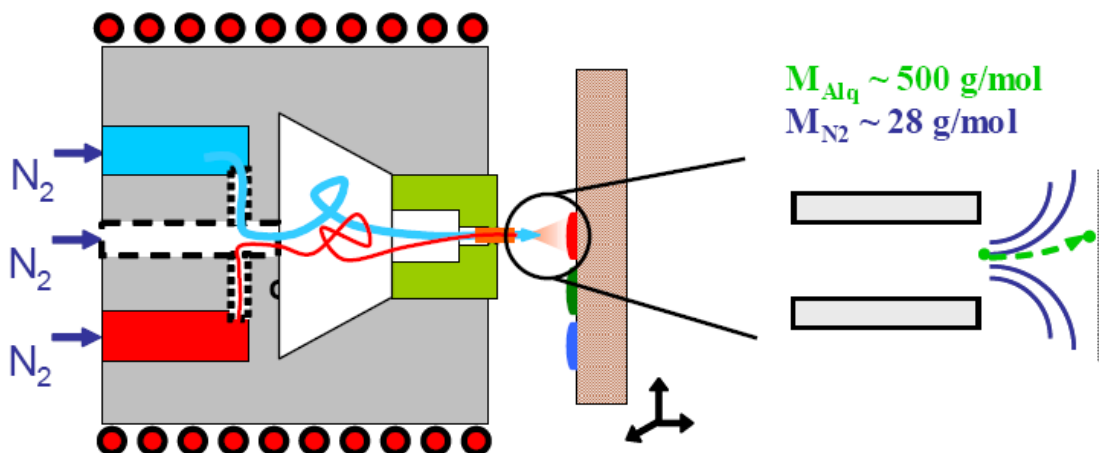


Figure 2.4: Schematic diagram of the organic vapor jet printing process [59].

- Shadow mask can only handle limited-size substrates.
- The resolution is limited by laser cutting process for defining features in stencil mask ( $> 100\mu m$ ).
- Alignment is problematic.
- The cost is high since it requires a vacuum process.

## 2.6.2 Organic Vapor Jet Printing

Organic vapor jet printing was developed by Stein et al. for small molecule patterning [59, 60]. A schematic of the organic vapor jet printing process is shown in Figure 2.4. In this method, organic molecules are sublimed into a hot inert carrier gas, which is then ejected through a microscopic nozzle onto a cooled substrate placed in proximity. As a result, a well-defined thin film is deposited on the substrate.

Advantages of the organic vapor jet printing include:

- It is a digital printing method which does not require any mask.
- It is an additive method so material use efficiency is high.

Disadvantages include:

- Resolution is low due to the dispersion of the jet stream out of the nozzle. In addition, the resolution also depends on the nozzle radius, nozzle-to-substrate separation, the deposition chamber pressure, and the masses of the carrier gas and organic molecules, etc.
- The deposited film is cone-shaped and so not uniform in thickness.
- The jet stream is usually continuous (in contrast to the “droplet-on-demand” capability in ink-jet printing). Thus it is difficult to print discrete pixels.

### 2.6.3 Molecular Jet Printing

Chen et al. introduced a molecular jet printing technique for vacuum deposition and patterning of small molecular OLED [12]. The apparatus used for the molecular jet printing method is illustrated in Figure 2.5. A print head is prepared with a MEMS shutter to control the flux by opening/closing the shutter. Small molecules are thermally evaporated in a flux and the print head controls the shutter status for selective deposition, assisted by an x-y stage. This process can be regarded as a “flux-on-demand” process for small molecules, similar to “drop-on-demand” of ink-jet printing for polymers.

The following features are related to this method:

- Similar to ink-jet printing, this method is a digital process which means no new mask is needed for a new design.
- This method is only good for small molecules.
- Although it is an additive process, the materials use efficiency may be low due to the fact that majority of the vapor flux is wasted.

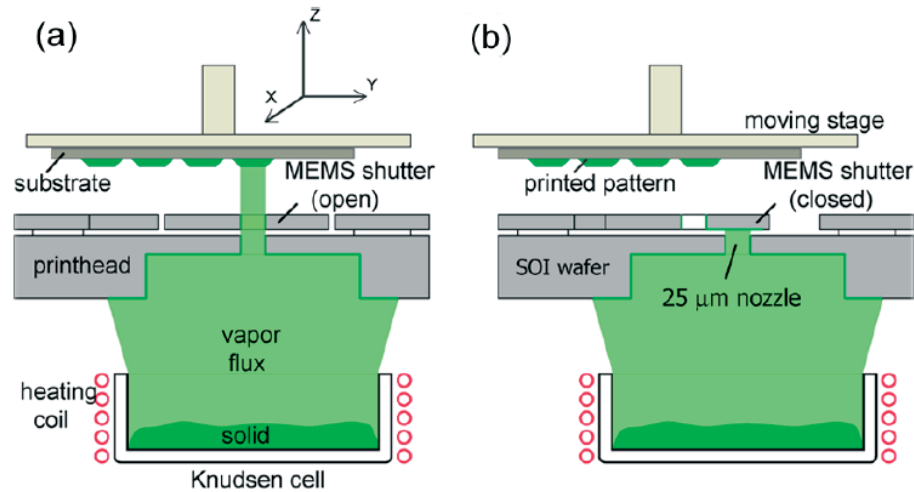


Figure 2.5: Illustration of the molecular jet printing apparatus and process [12]. (a) Shutter is open (b) Shutter is closed.

- The resolution is higher than for the shadow-mask evaporation method.
- The cost is high since it requires a vacuum process.
- The throughput is extremely low, since it is a serial process and the evaporation rate for the deposition of each pixel is usually kept low.
- It has the potential to scale to large substrates but the cost and throughput would be a big concern.

#### 2.6.4 Small-Molecule Stamping

In this method, multi-layer stacks of small molecules are evaporated onto a stamp surface and the whole stack is then transferred onto device plate [13]. Figure 2.6 shows a schematic diagram of the small molecules stamping process. By repeating the process with R, G and B subpixels a full-color OLED display can be made in principle, although it has not yet been demonstrated [13]. This method is believed to have high resolution and can be used for patterning of small molecules. One concern

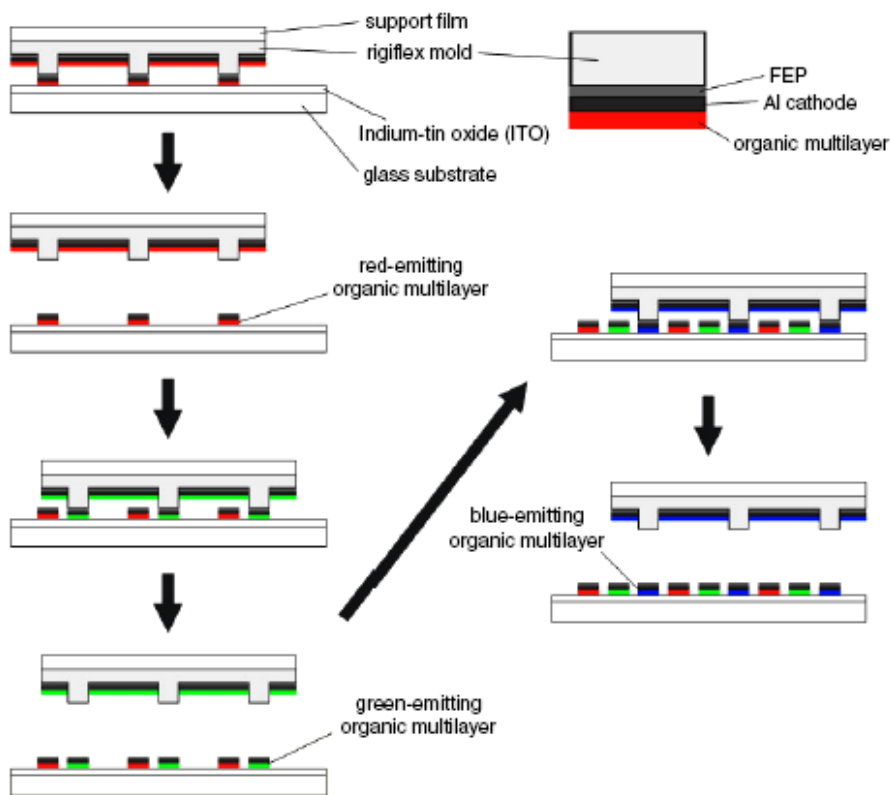


Figure 2.6: Schematic diagram of the small-molecule stamping process [13].

related to this method is that contact contamination might present which will affect the device performance.

## 2.7 Outlook

This chapter reviewed several patterning methods that have been invented for organic layer patterning used for the fabrication of OLED displays. As discussed in this chapter, however, there are still challenges to be solved before any particular patterning method will stand out and will make low-cost OLED display manufacturing possible. To develop new patterning methods that would be practical is the focus of this thesis. Throughout the thesis, we have developed three new patterning techniques.

In Chapter 3 the material system, device structure, general fabrication and testing procedures, etc. is described.

In Chapter 4 a Large-Area Wet Micro-Printing (LAMP) method is described. This LAMP method is somewhat similar to offset printing. In this method a printing plate with a surface energy pattern is first prepared. The printing plate can thus pick up ink droplets (light-emitting polymer solution) and these droplets can further be transferred onto a device plate by a contact and separation step. After solvent evaporation, a light-emitting polymer thin film will be left in predefined locations. By repeating these steps three times for different colors, a R, G, B subpixel array can be deposited. This method should be able to handle large area substrates. It is a wet printing process and in principle could be very fast. It also has the potential to evolve into a roll-to-roll printing technology. Since all wet-printing methods generally lead to a non-uniform film thickness, two approaches are utilized in this thesis to optimize the wet-printed film profile, which are discussed in detail in Chapter 5.

In Chapter 6 a transfer printing method is introduced. This transfer printing method is a dry printing method. The basic idea of the method is that a uniform dry film of the materials to be patterned is first formed on a soft substrate. A hard stamp is pressed onto the dry film to locally rupture the film. Upon stamp separation, positive and negative patterns will be formed on both the stamp side and the substrate side, respectively, thanks to the adhesion difference. The pattern formed is then transfer printed again onto a device plate. By repeating these steps for different color emitting materials, it is possible to realize full-color OLED display patterning. This method is able to achieve very high resolution and very uniform film thickness, and is thus a promising patterning technique for future OLED display manufacturing.

A similar transfer printing method is also discussed in Chapter 7. In this method, the stamp is the same as the first transfer printing method discussed in Chapter 6. However, the polymer film to be patterned is directly spin-coated onto the stamp surface. Due to the protrusions of the stamp surface the spin-coated layer is naturally

discontinuous. By surface energy treatment of the stamp surface, this layer can be transferred onto device plates as well. In a similar step and repeat way, full-color OLED subpixels could be deposited. This transfer printing method has reduced processing steps compared with the first transfer printing method and thus could further reduce the manufacturing cost.

# Device Fabrication

Specific fabrication processes pertaining to patterning will be described in detail when used in later chapters. However, some of the processing steps are common to all fabricated devices or are used for the fabrication of control devices. For convenience, a standard OLED process is briefly outlined here for later reference. The standard procedures have been used by former students in our group [54, 66, 67].

### 3.1 Substrate and Anode

A “standard” OLED used in this thesis has a basic structure shown in Figure 3.1. Indium-tin oxide (ITO) is used as the anode for the OLED. Glass substrate pre-coated with ITO was purchased from Colorado Concept Coatings LLC. The substrate is 1.1-mm-thick polished soda lime float glass and the ITO coating layer is about 150 nm with a measured sheet resistance of 9–15  $\Omega/\square$ .

When necessary, the blanket ITO film can be patterned by wet etching with photoresist as mask. The etch solution is formed with 10 parts of DI-water with 9 parts of HCl and 1 part of HNO<sub>3</sub>. The etch is done at a temperature of 40–60°C on a hotplate. For the ITO layer used in our experiments, the etch time is about 3 minutes at 45°C, but different batches differ slightly. After the etch a multi-meter is used to check the conductivity to ensure the complete removal of ITO in the etch

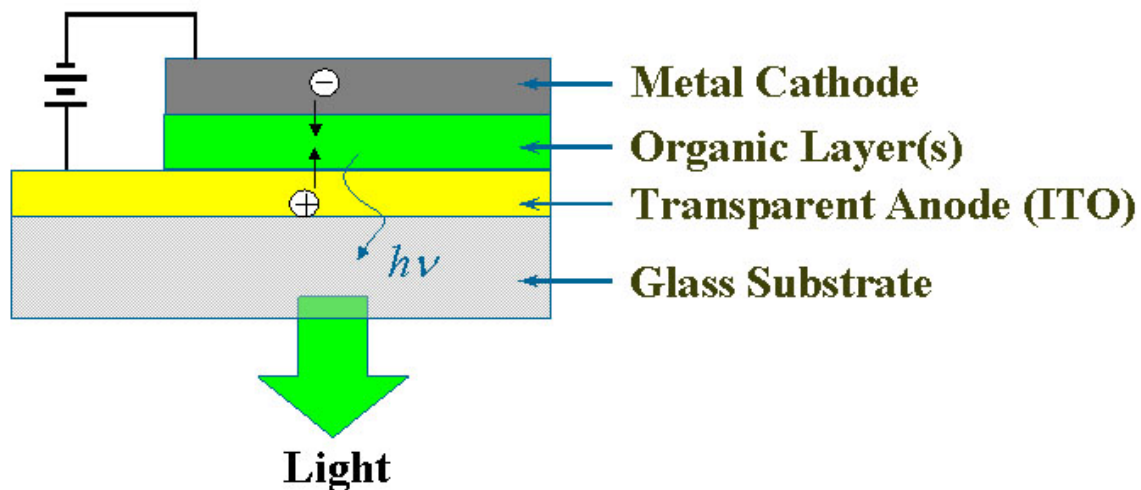


Figure 3.1: Structure of a standard OLED

region.

The following steps are used in order to clean the ITO surface:

1. DI-water bath with detergent Micro-90 heated to boil, then ultrasonic clean for 1 hour.
2. Rinse in DI-water, then blow dry with nitrogen gas.
3. Solvent cleaning with chloroform.
4. Solvent cleaning with acetone.
5. Solvent cleaning with isopropanol.
6. Blow dry with nitrogen gas.

A short oxygen plasma treatment is performed on the ITO surface right before the spin-coating of any polymer layers to raise the work function energy of the ITO [68]. The oxygen plasma treatment is done with a PlasmaTherm 720 with the following parameters: pressure at 150 mTorr, oxygen flow at 25 sccm, power at 25 W, processing time for 4 minutes.

## 3.2 Light Emitting Layer

In this thesis work, we focus our work on polymer-based OLEDs, so we are mostly working with polymer light-emitting layers. Figure 3.2 lists the chemical structures of various organic compounds used in this thesis. Poly(N-vinylcarbazole) (PVK) is used as the host polymer and hole-transport polymer. The chemical structure of PVK is shown in Figure 3.2a. Unlike other conjugated polymers (such as poly(p-phenylene vinylene), PPV) with alternating single and double bonds, PVK has a fully saturated backbone. The optical and electrical characteristics of PVK are mainly defined by the carbazole side-groups attached to the inactive backbone. The PVK used in this work was obtained from Sigma-Aldrich, having a molecular weight of  $M_w = 1,100,000$  g/mole and a glass transition temperature of  $T_g = 200^\circ\text{C}$ . To assist electron-transport, small molecule 2-(4-Biphenyl)-5-(4-tert-butyl-phenyl)-1,3,4-oxadiazole (PBD, Figure 3.2b), purchased also from Sigma-Aldrich, was added to PVK to form a mixture. The mixture was dissolved into solvent (usually chlorobenzene) to form a solution for film formation. In addition to PVK and PBD, small amount of laser dyes are used to tune the color emission. Three different laser dyes are used in this work. They are coumarin 6 (C6, Figure 3.2c) for green, Nile red (Figure 3.2d) for red and coumarin 47 (C47, Figure 3.2e) for blue. The green dye C6 and blue dye C47 were obtained from Lambda-Physik and Nile red was purchased from Sigma-Aldrich. Figure 3.3 shows the normalized electroluminescence spectra for PVK/PBD devices doped with different dyes. Emission spectra were measured with a spectrometer (Photo Science 650).

Chlorobenzene is used as the solvent. PVK, PBD and one kind of dye are mixed and dissolved in chlorobenzene to form a solution. The following weight ratios (PVK:PBD:dye) for optimal device performance were used, based on previous results [68]: PVK:PBD:C6 = 100:40:0.3, PVK:PBD:Nile red = 100:40:0.2, PVK:PBD:C47 = 100:40:1. Each mixture (with 100 mg PVK and 40 mg PBD and

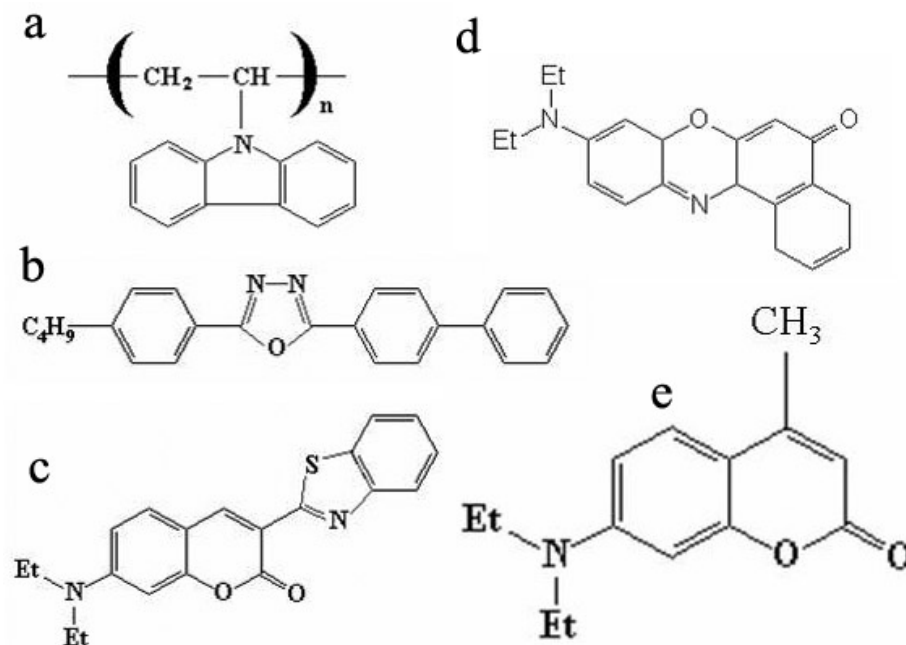


Figure 3.2: Chemical structures of various compounds used in this thesis. (a) PVK host polymer acting as hole transport layer, (b) PBD for electron transport, (c) green dye C6 (d) red dye Nile red, (e) blue dye C47.

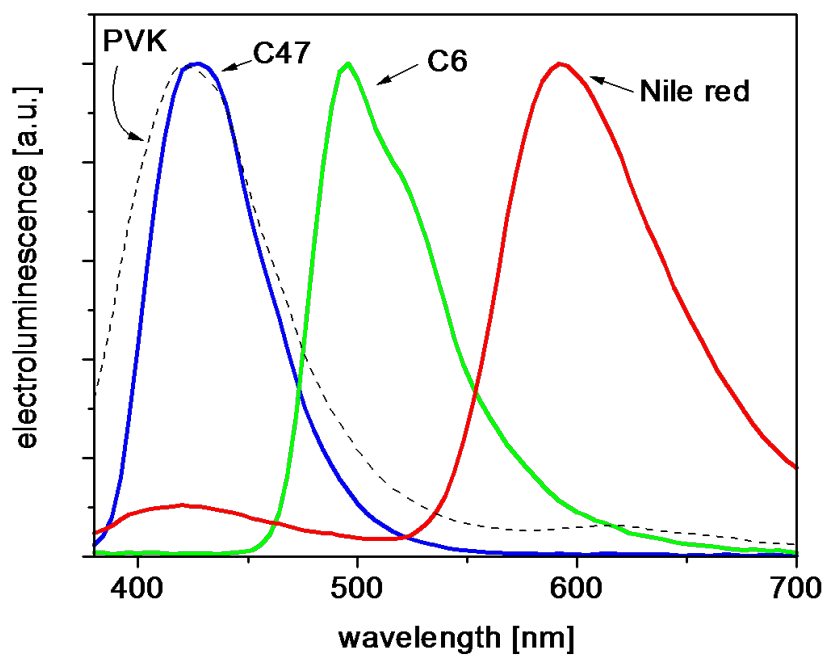


Figure 3.3: Electroluminescence spectra of standard PVK/PBD devices doped with C47, C6 or Nile red [54].

the appropriate amount of dye) is dissolved into 7.5 ml chlorobenzene. The mixture is stirred with a magnetic bar until the polymer is fully dissolved. A disposable syringe with 0.2  $\mu\text{m}$  filter is used to filter the stirred solution. The resulting solution is then used to form the film by spin coating on the ITO-coated glass substrate. The film thickness depends on spin speed, spin time and the concentration of the polymer mixture in the solvent used, etc. For the solution mentioned above, a spin speed of 2000 rpm for 50 seconds yields a film of  $\sim 70\text{--}100$  nm thick.

### 3.3 Cathode

Following spin coating of the polymer layer, the device is promptly transferred into a high-vacuum thermal evaporator (Ångstrom Engineering) with 4 independently controllable sources. An alloy of magnesium and silver is used as the cathode, co-deposited from two independent sources. Silver is used here mainly to slow the atmospheric corrosion of the otherwise very active component: magnesium. The film is deposited with an evaporation rate of  $6\text{Å}/\text{sec}$  for magnesium and  $0.6\text{Å}/\text{sec}$  for silver, resulting in a film of approximately 10 parts of magnesium to 1 part of silver.<sup>1</sup> The total thickness of the Mg:Ag film is  $500\text{ Å}$ . Another silver layer ( $500\text{ Å}$ ) is deposited as a capping layer to protect the Mg:Ag layer from corrosion. In order to make discrete OLEDs, in most cases the metal is evaporated through a shadow mask to form the desired pattern. The most frequently used shadow mask has openings of  $2\text{ mm}^2$ .

### 3.4 Device Test

After the cathode evaporation, the finished sample is transferred into a glove box for testing. A probe station with a microscope and micro-manipulators is used for

---

<sup>1</sup>For silver evaporation, add new silver shots when necessary. For magnesium evaporation, discard old magnesium shots and replenish with fresh shots after every two runs to ensure a good quality cathode layer.

the test. One probe is needed to make contact with the ITO anode and another for the metal cathode. The soft polymer film is easily scratched off by the probe tip, so one can easily make contact with the ITO layer. On the other hand, it is easy to accidentally punch through the metal cathode layer to the ITO below and cause short-circuited devices. Previously a thin gold wire (0.001" diameter) was soldered onto the probe tip to make the contact with metal. From my experience, it is difficult to solder a thin gold wire to the probe tip for a reliable contact. In this work, a special kind of flexible probe tip was used (Creative Devices Inc., model 72F-B5/05). The sharp and flexible tip is further bent with tweezers to form a small curvature at the tip. The probe with modified flexible tip is able to make consistent and reliable contact to the metal cathode without punching through the metal electrode. We use an Agilent 4155C semiconductor parameter analyzer to measure the current-voltage (I-V) characteristics of the device. A 10-mm-diameter silicon photo-detector (PIN-10DP from UDT Sensors, Inc.), in close proximity to the OLED was used to measure the light output. The light output was converted to photocurrent  $I_{ph}$  and was recorded by the Agilent analyzer simultaneously. For most experiments done in this work, the photocurrent data is sufficient to compare relative device performance since all devices are measured with the same testing apparatus.

Figure 3.4 is a photo of the testing setup within the glove box. Shown on the image are the photodiode and its cable which connects to the parameter analyzer, the microscope and micro-manipulators with probe tips. The OLEDs under test were to be placed directly on top of the holder that holds the photodiode.

For comparison to devices from other groups, however, external quantum efficiency  $\eta_{ext}$ , defined as the ratio of externally collected photons and injected electrons, can be calculated from the following two equations:<sup>2</sup>

---

<sup>2</sup>In reality, both the emission spectra (Figure 3.3) and the photodetector spectra response  $R(\lambda)$  (Figure 3.5) are functions of wavelength  $\lambda$ . In order to calculate the external quantum efficiency a

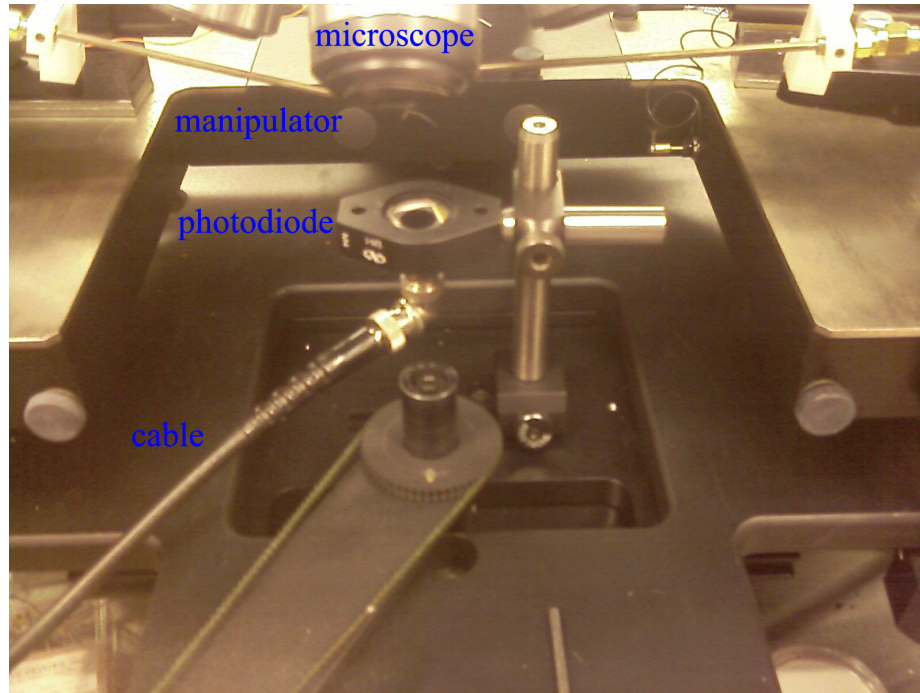


Figure 3.4: A photo of the testing setup, including the photodiode and a cable leading to the parameter analyzer, the microscope and micro-manipulators with probe tips.

$$\eta_{ext} = \frac{Q(\lambda)/(hc/\lambda)}{I_{OLED}/e} \quad (3.2)$$

$$I_{ph} = G \cdot R(\lambda) \cdot Q(\lambda) \quad (3.3)$$

Where,

$\eta_{ext}$ : external quantum efficiency, dimensionless

$Q(\lambda)$ : total optical output power, unit W

$h$ : Planck's constant

$c$ : speed of light

more sophisticated approach would have been used, which contains an integral.

$$I_{ph} = \int G \cdot R(\lambda) \cdot Q(\lambda) d\lambda \quad (3.1)$$

A simplified approach is to assume that all light was emitted at the wavelength of peak intensity for easy calculation. A small error is introduced but this is a good approximation.

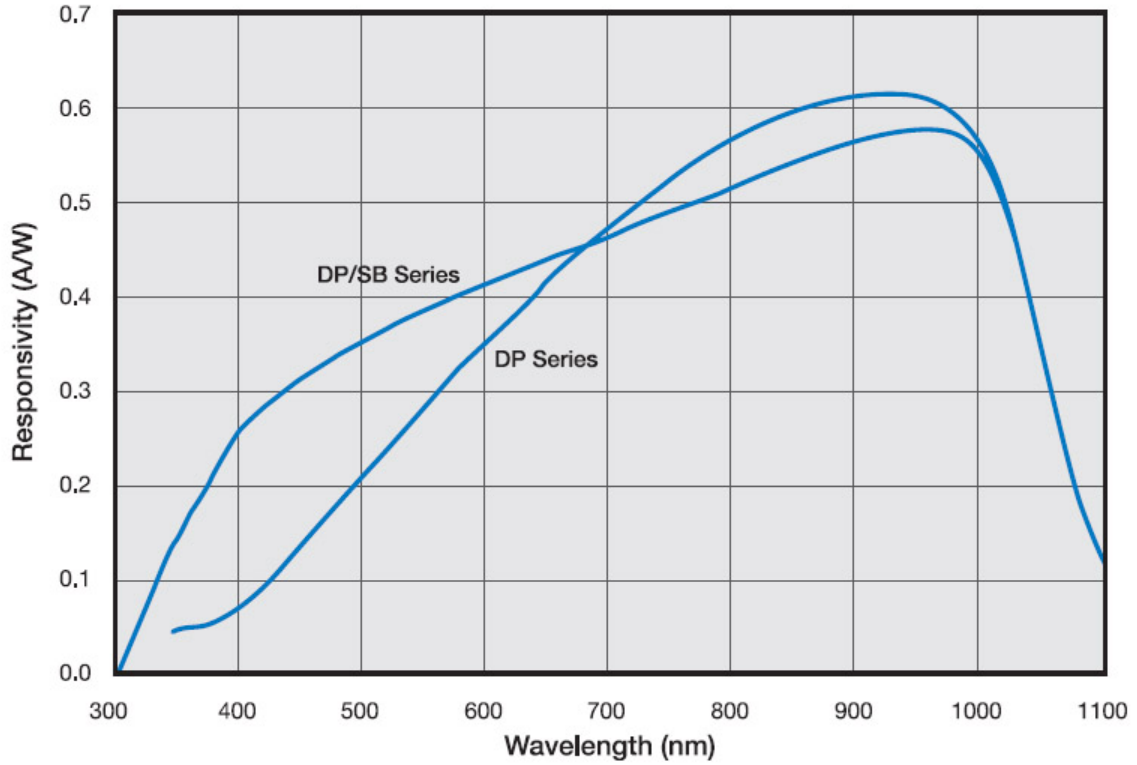


Figure 3.5: Photodetector response spectra for PIN-10DP (DP series) from UDT Sensors, Inc.

$\lambda$ : photon wavelength, unit meter

$I_{OLED}$ : OLED current, unit A

$I_{ph}$ : measured photocurrent from the photodetector, unit A

$G$ : light collection efficiency, dimensionless

$R(\lambda)$ : the responsivity of the photodetector (Figure 3.5), unit A/W

This leads to the following expression:

$$\eta_{ext} = \frac{e \cdot \lambda}{h \cdot c \cdot G \cdot R(\lambda)} \cdot \frac{I_{ph}}{I_{OLED}} = F_{conv} \cdot \frac{I_{ph}}{I_{OLED}} \quad (3.4)$$

Where  $F_{conv}$  is a conversion factor for a given electroluminescence spectrum and a given setup. For our setup the light collection efficiency  $G$  is estimated to be 70%.

The value of the conversion factor  $F$  for different dyes is given in Table 3.1 [54].

In addition, the luminance  $L$  (defined as the luminous intensity per unit area of

Table 3.1: Conversion factor  $F_{conv}$  for different dye OLED [54]

Dye (peak wavelength)	$F_{conv}$
C47 (420 nm)	279
C6 (495 nm)	220
Nile red (600 nm)	188

light traveling in a given direction, unit  $cd/m^2$ ) of the device can be calculated with:

$$L = \frac{C(\lambda) \cdot Q(\lambda)}{Area \cdot 2\pi} \quad (3.5)$$

Where  $C(\lambda)$  is photopic luminous efficiency (unit lm/W). For example, for a green emitter at 500 nm,  $C(\lambda = 500nm) = 410$  lm/W.

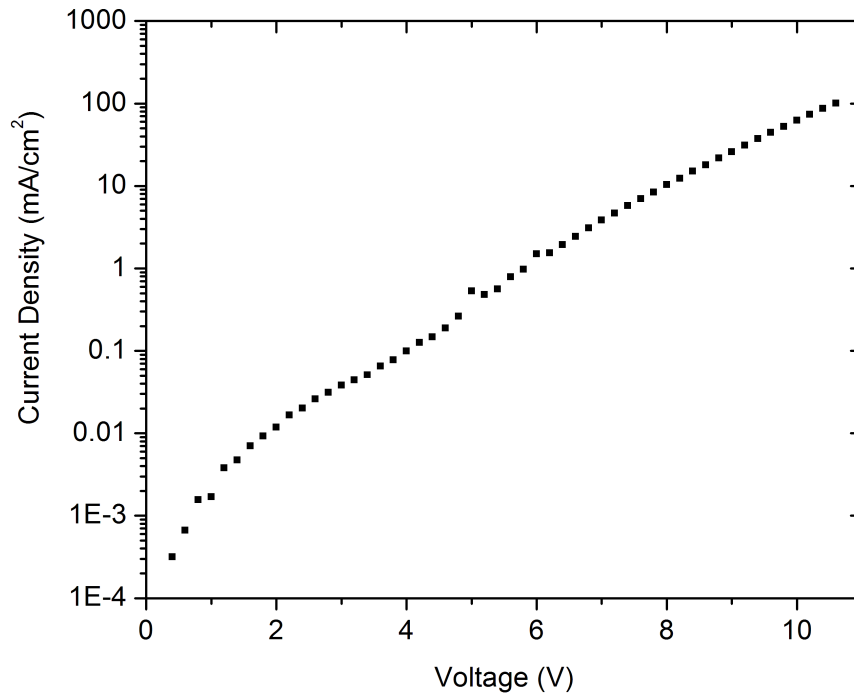
$Area$  is the device area, unit  $m^2$

The factor  $2\pi$  (solid angle of half sphere) arises from the assumption that the emission vs. angle dependence of the OLED follows a Lambertian shape.

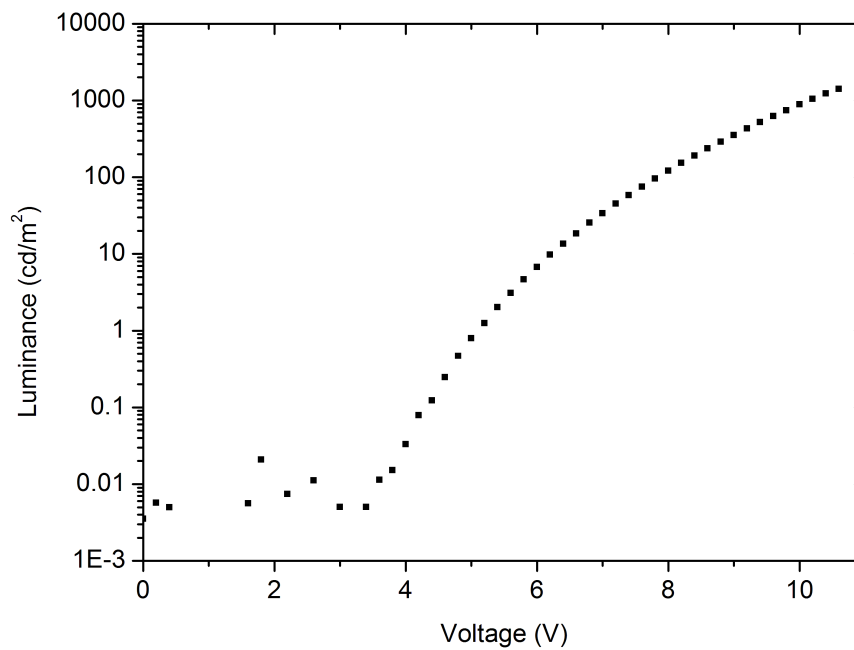
The luminous efficiency  $\eta_L$  (unit cd/A) of an OLED can be calculated with:

$$\eta_L = \frac{L}{I_{OLED}/Area} \quad (3.6)$$

Some typical examples of the performance of PVK:PBD:C6 OLED fabricated as described in Section 3.1-3.3 are shown in Figure 3.6.

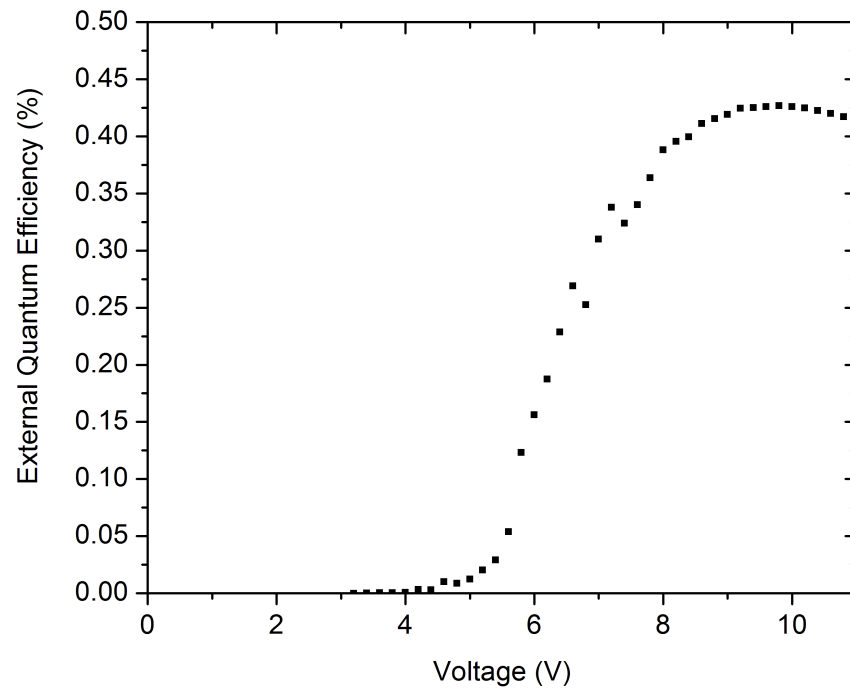


(a) Current vs. voltage curve

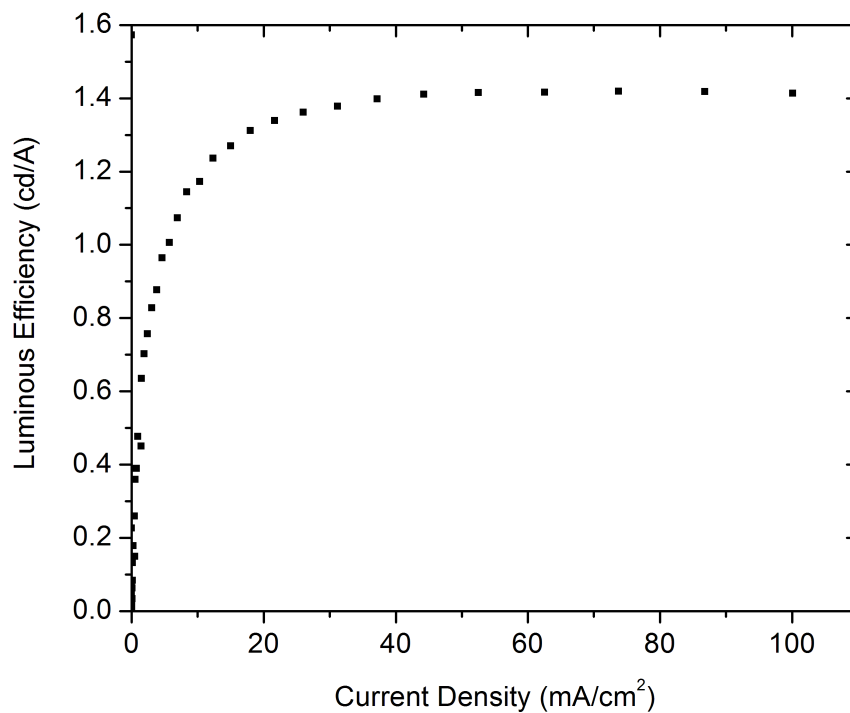


(b) Luminance vs. voltage curve

Figure 3.6: Various OLED curves from a typical PVK:PBD:C6 OLED fabricated as described in Section 3.1-3.3.



(c) External quantum efficiency vs. voltage curve



(d) Luminous efficiency vs. current density curve

Figure 3.6: Various OLED curves from a typical PVK:PBD:C6 OLED fabricated as described in Section 3.1-3.3. (cont'd)

# Large-Area Wet Micro-Printing

As discussed in Chapter 2 Section 2.1, ink-jet printing has been widely developed for the patterning of light-emitting polymers for OLEDs. Nevertheless, there are several shortcomings to ink-jet printing, such as profile uniformity of the dried film, nozzle clogging, repeatability of the direction of droplet travel, and throughput.

In this chapter a novel printing approach is demonstrated [31], which prints organic device layers from a wet solution not drop by drop, as in ink-jet printing, but rather over a large area at once using a patterned printing plate. We refer to the method as Large-Area wet Micro-Printing (LAMP). This method uses surface engineering techniques to pattern the surface energy of a printing plate and then uses the printing plate to locally deposit organic materials. Patterning of different color pixels for a full-color OLED display can be achieved by three successive printing steps.

Both single-color pixel arrays and R, G, B sub-pixel arrays are demonstrated. Monochrome OLED devices were tested for their electrical and electroluminescent properties. The printed devices show efficiencies somewhat lower than but close to those by spin-coating without any optimization. The results suggest that LAMP is a promising patterning technique for low-cost full-color OLED displays.

The information in this chapter was presented in Ref. [31, 32].

## 4.1 Concept of Large-Area Wet Micro-Printing

The concept of the LAMP printing process is shown schematically in Figure 4.1. A printing plate is first prepared by surface energy patterning (discussed later) so that a designed wettability pattern is achieved. The printing plate is then coated with “inks”, a solution with dissolved organic materials (e.g., red light-emitting polymer) to be printed. Guided by the wettability pattern, the inks stick only to selected regions of the printing plate. The printing plate is then brought into contact with the device substrate, during which inks are transferred to desired locations. Following printing, the printing plate is separated from the contact with the device plate and the solvent is allowed to dry, leaving a patterned organic film on the target substrate. Finally, repeating the previous steps for the green and blue light-emitting polymers required for a full-color OLED display completes the LAMP process.

The concept may look similar to that of Darhuber et al. [14] and Miller et al. [50], for printing single polymer layer, but differs in the fact that they printed polymers either in their precursor form [14] or above  $T_g$  [50], not polymers in solution. In addition, only passive polymers were printed (prepolymer of polyurethane and polystyrene) in single layer in their work. In our work, light-emitting layers are printed in a multi-step structure (side-by-side), which is aimed at full-color OLED display applications.

## 4.2 Surface Energy Patterning of the Printing Plate

As can be seen from last section, one important process in the LAMP method is the preparation of the printing plate. The basic requirement of the printing plate is to have patterned wettability so that it can be selectively coated with inks.

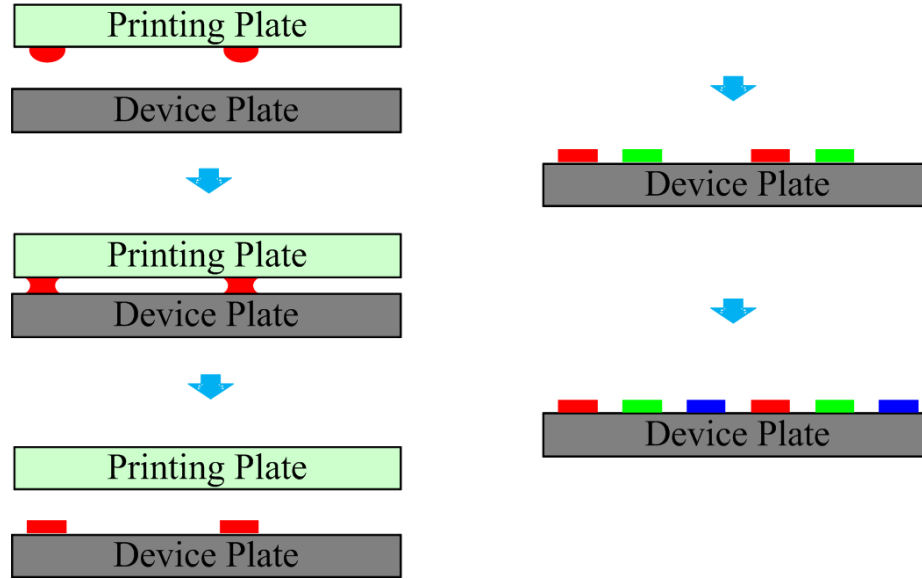


Figure 4.1: Schematic diagram of Large-Area wet Micro-Printing (LAMP) technique for organic device patterning. a) a surface-energy-patterned printing plate is coated with red “ink”; b) the printing plate is brought into contact with the device plate, i.e., to print; c) the printing plate is separated from the device plate and the transferred “ink” is allowed to dry; d,e) steps a-c are repeated for green and blue sub-pixels.

### 4.2.1 Wettability

Wetting is the ability of a liquid to maintain contact with a solid surface. Wettability (the degree of wetting) is determined by a force balance between adhesive and cohesive forces. Wettability is usually characterized by the contact angle  $\theta$  at which a liquid/vapor interface meets the solid surface. As shown in Figure 4.2, when a small liquid droplet is put on a flat solid surface, two distinct wetting regimes may be found: partial wetting and complete wetting. On Figure 4.2a and 4.2b the liquid droplets form finite contact angles  $\theta_e^1$ , which corresponds to partial wetting. On Figure 4.2c the contact angle  $\theta_e = 0$ , which corresponds to complete wetting.

In equilibrium the three (solid, liquid and vapor) phases are in contact at the contact line, i.e., the liquid phase of the droplet (L), the solid phase of the substrate (S), and the vapor phase (V). The theoretical description of contact arises from the consideration of a thermodynamic equilibrium between the three phases, which gives

<sup>1</sup>The subscript e in  $\theta_e$  refers to an equilibrium property.

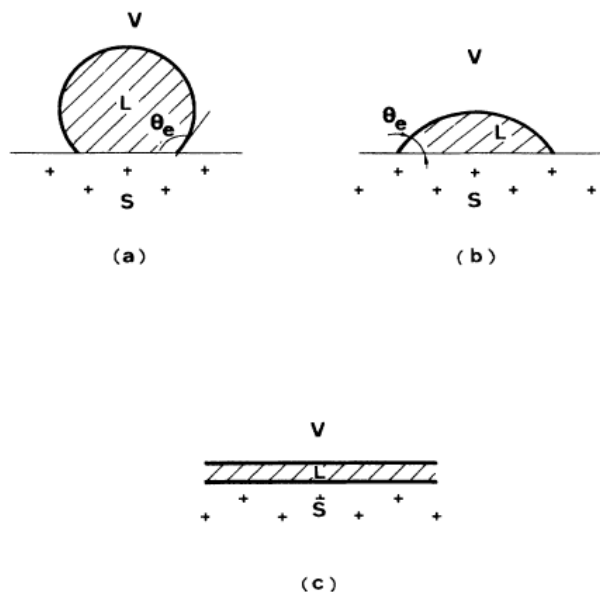


Figure 4.2: A small droplet in equilibrium over a horizontal surface: (a) and (b) correspond to partial wetting, the trend towards wetting being stronger in (b) than in (a). (c) corresponds to complete wetting ( $\theta_e = 0$ ) [17].

the following equation, known as the Young's equation [17]:

$$\gamma_{SV} - \gamma_{SL} - \gamma \cos \theta_e = 0 \quad (4.1)$$

Where  $\gamma_{SV}$  refers to the solid-vapor interfacial energy,  $\gamma_{SL}$  refers to the solid-liquid interfacial energy.  $\gamma_{LV}$  refers to the liquid-vapor energy and is equal to the surface tension of the liquid, and is usually designated simply as  $\gamma$ .

### 4.2.2 Zisman Plot

From the Young's equation, wettability depends on both the surface tension of the liquid and the difference  $\gamma_{SV} - \gamma_{SL}$ . While the liquid surface tension can be easily measured, the term  $\gamma_{SV} - \gamma_{SL}$  is a value based on both the property of the solid and the specific liquid used and is in general not directly measurable.

An alternative way to gain understanding of the solid surface can be obtained by a

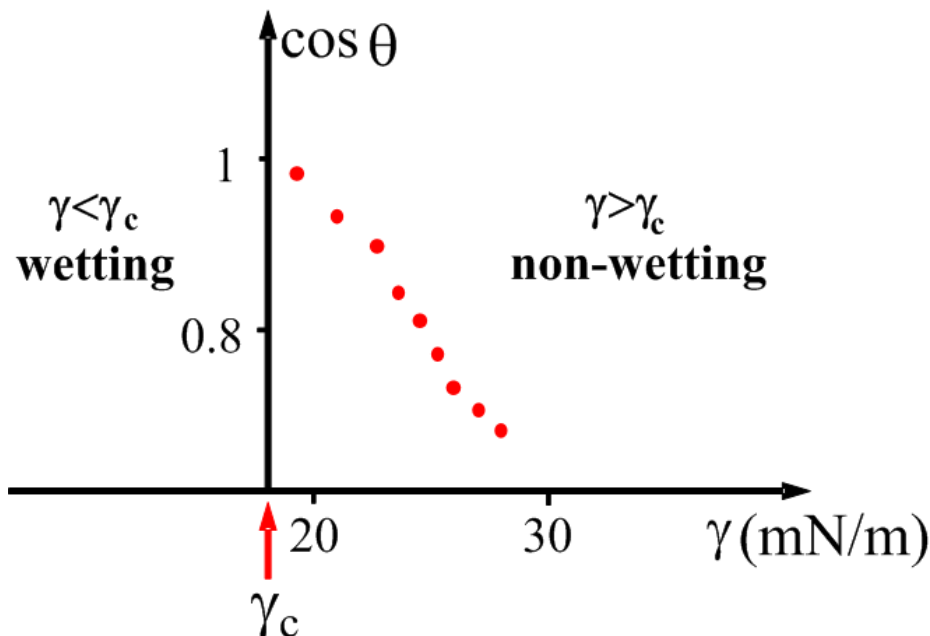


Figure 4.3: A typical Zisman plot for a Teflon surface in contact with n-alkanes liquids (modified from [20]). The critical surface energy  $\gamma_c$  for this system is about 18 mN/m.

Zisman plot. By using a series of homologous liquids (n-alkanes for example), Zisman studied the contact angles on a given solid. Zisman observed that  $\cos\theta$  increases as the surface tension of the liquid  $\gamma$  decreases. He then plotted  $\cos\theta$  versus the surface tension of the liquids  $\gamma$ . A typical Zisman plot is shown on Figure 4.3. By a linear extrapolation, he defines the value  $\gamma_{\cos\theta=1}$  or  $\gamma_{\theta=0}$  (for complete wetting) as the critical surface tension of the given solid  $\gamma_c$ .

In general,  $\gamma_c$  would depend on both the properties of the given solid, and on the properties of the liquid series used for the experiments. However, Zisman observed that  $\gamma_c$  is essentially independent of the nature of the liquid and is thus a characteristic of the solid alone. For example, the solid surface used for the Zisman plot shown on Figure 4.3 is Teflon. From Figure 4.3,  $\gamma_c$  of Teflon is estimated to be  $\sim 18$  mN/m. In other words, a liquid (with surface tension  $\gamma$ ) will completely wet the solid if  $\gamma < \gamma_c$ . Otherwise incomplete wetting (or partial wetting) occurs if  $\gamma > \gamma_c$ .

### 4.2.3 High Energy vs. Low Energy Surfaces

There are two main types of solid surfaces: high energy surfaces (large  $\gamma_c$ ) and low energy surfaces. The relative energy of a solid is related to the bulk cohesive energy of the solid itself. Hard solids (covalent, metallic or ionic, e.g., metals, glasses and ceramics) are usually high energy surfaces, while weak molecular crystals (bonded by van der Waals forces or hydrogen bonds, e.g., fluorocarbons, hydrocarbons, etc.) are usually low energy surfaces.

For our LAMP method, the printing plate is made from a silicon wafer for convenience. A silicon wafer (with a native oxide layer) has a very high surface energy, i.e., it will be wetted by most liquids. Thus a way to modify the silicon surface to lower its surface energy must be used in order to have selective wettability.

### 4.2.4 Fluorinated Surface

There are many different ways to modify a surface in order to change its surface energy or wettability. A common way is to coat the high-energy surface with low-energy self-assembled layer.

Alkyl-trichlorosilane (with the form  $\text{RSiCl}_3$ , R denoting a hydrocarbon chain), for example, reacts with the hydroxyl groups on silicon oxide and forms a self-assembled layer, which has fairly low surface energy due to the  $\text{CH}_x$  groups [65].  $\text{CF}_x$  (found in Teflon) groups have even lower surface energies compared to  $\text{CH}_x$  groups. Thus, by replacing as many  $\text{CH}_x$  as possible with  $\text{CF}_x$ , the resulting perfluorinated alkyl-trichlorosilanes are found to be the most effective reagents to produce low-energy coatings on oxide-coated surfaces [5]. For example, layer formed from 1H,1H,2H,2H-perfluorodecyl-trichlorosilane ( $\text{CF}_3(\text{CF}_2)_7(\text{CH}_2)_2\text{SiCl}_3$ ) has a critical surface tension as low as 6 mN/m, in comparison to 15–18 mN/m for Teflon and 22–24 for alkyl-trichlorosilane-based self-assembly layers [8, 17].

In this work, 1H,1H,2H,2H-perfluorooctyl-trichlorosilane ( $\text{CF}_3(\text{CF}_2)_5(\text{CH}_2)_2\text{SiCl}_3$ ,

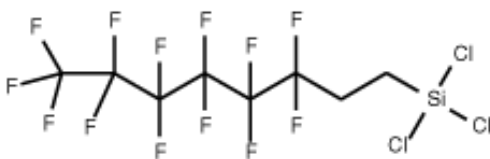


Figure 4.4: Schematic diagram showing the chemical structure of PFOTS.

PFOTS, purchased from Fluka) is used to adjust the surface energy of the printing plate [15]. Figure 4.4 shows the chemical structure of PFOTS. PFOTS forms a self-assembled layer on the  $\text{SiO}_x$  surface. The binding nature of the PFOTS layer is believed to be similar to the illustration given in Figure 4.5, i.e., the silicon atom in  $\text{RSiCl}_3$  forms one or two bonds to surface hydroxyl groups while the remainder of the Si-Cl bonds are hydrolyzed and a Si-O-Si linkage is formed between adjacent silanes [65]. Figure 4.5 is a simplified illustration of the silane layers on the surface. The actual structure may contain multilayers of silanes, because the Si-O bonds provide the possibility of crosslinking. Small amount of water content in the solution is preferred for the growth condition. If extra amount of water is present, however, PFOTS precursor molecules will tend to bond to each other and thus form aggregations rather than attach to the substrate.

Since the PFOTS has a very low critical surface tension, the surface becomes hydrophobic and can de-wet most liquids. On the contrary, a clean silicon dioxide surface has a very high surface energy and is thus wettable for most liquids. Thus, we are able to prepare two surfaces with extremely different surface energies or wettabilities.

For convenience, surface tension of commonly used liquids and critical surface tensions of some substrates are listed in Table 4.1.

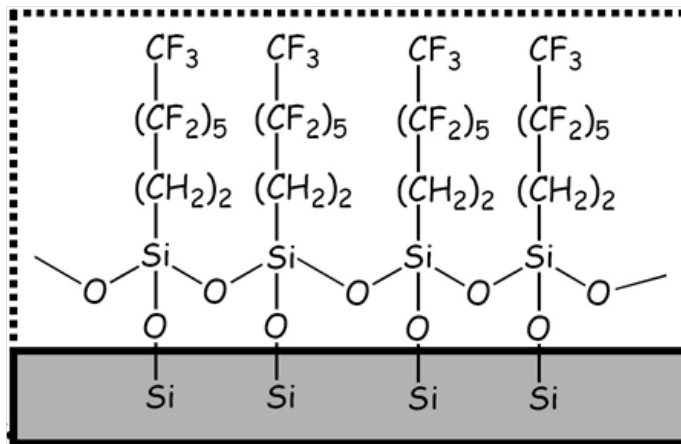
Figure 4.5: One possible structure of the PFOTS layer formed on a  $\text{SiO}_x$  surface.

Table 4.1: Surface tensions of commonly used liquids and substrates

Liquids/Substrates	Surface Tension, mN/m
Chlorobenzene	33
Chloroform	27
Dimethyl sulfoxide (DMSO)	48
Ethylene glycol	48
Glycerol	64
Water	72
Alkyltrichlorosilane	~22–24
Glass	~1000
PFOTS	~6
Teflon	12

### 4.2.5 Printing Plate Fabrication

The printing plate used here was prepared by combining photolithography with molecular self-assembly of the PFOTS. The procedures used for the fabrication of the printing plate is illustrated in Figure 4.6. A silicon wafer is first patterned with a photoresist layer by conventional photolithography.

As has been pointed out earlier, a very small amount of water content is preferred for the growth of the PFOTS, while an excess amount of water is harmful to the growth. In our experiments, the PFOTS growth on the wafer is done in a nitrogen glove box with controlled moisture (less than 10 ppm). In addition, anhydrous (99%+) dodecane is used as the solvent. The silicon wafer with the patterned photoresist layer is baked for 10~20 minutes at 120°C and then immersed into dodecane solution for five minutes in a glove box. After that, a few drops of PFOTS molecules are added to the dodecane solution (the PFOTS concentration is estimated to be a few mM). No stirring or shaking is necessary. The plate is kept in the solution for 20 minutes and then removed from the solution and taken out of the glove box and rinsed in de-ionized water and blown dry. A PFOTS layer will form on the surface where there is no photoresist. Extra PFOTS molecules or aggregations are removed by the rinse. Finally the photoresist is stripped off by acetone in an ultrasonic bath. The printing plate is thus fabricated, containing both high surface energy (clean surface region) and low surface energy (PFOTS-coated) regions. In order to limit the absorption of water, the use of acetone and isopropanol is limited. Instead, trichloroethylene is used to wash the glass dish container.

In our experiments glass substrates are also used and the procedures used for the fabrication of printing plates from a glass substrate is the same as from a silicon wafer. Once printing plates are fabricated, the surface energy pattern can be shown by dip-coating of the surface by various liquids. Some of these tests are shown in Figure 4.7.

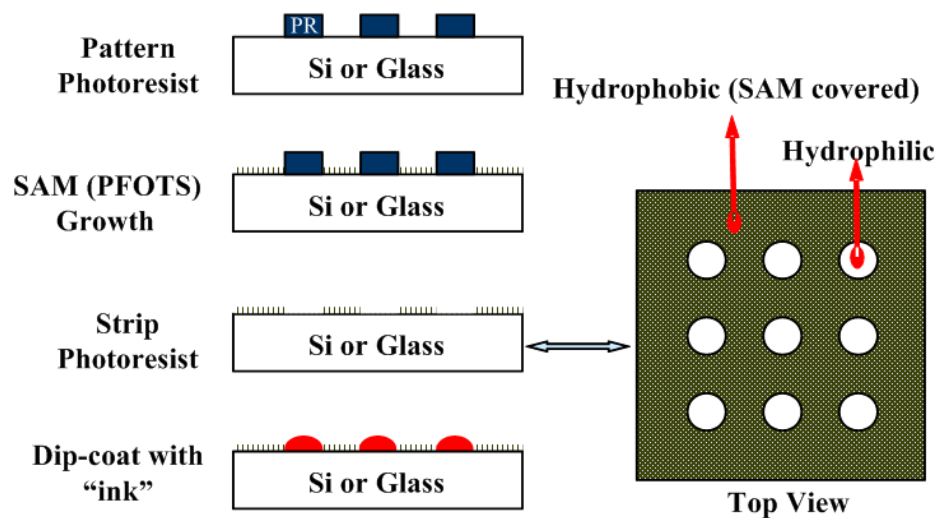
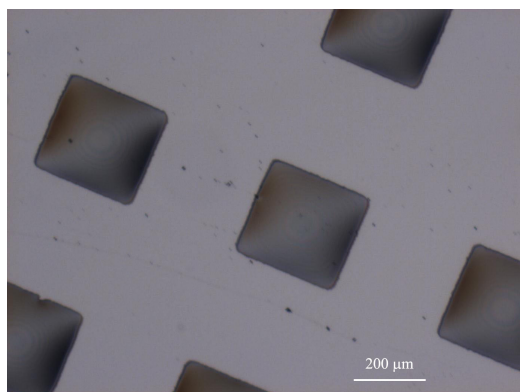
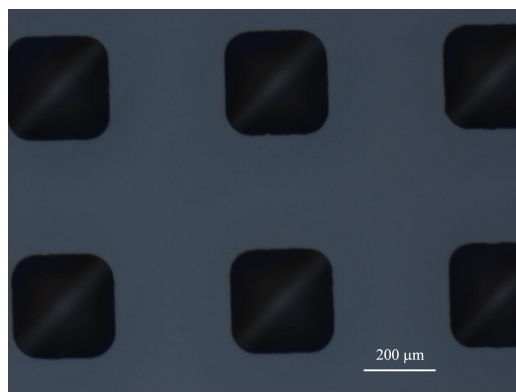


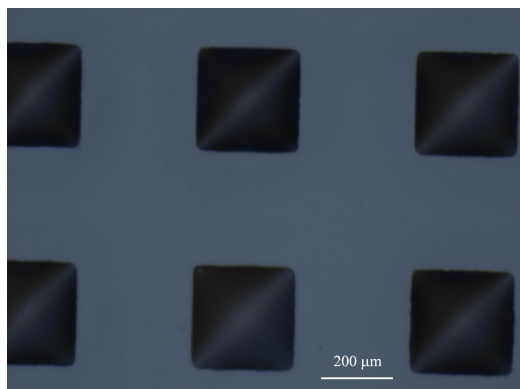
Figure 4.6: Procedures used for the fabrication of the printing plate.



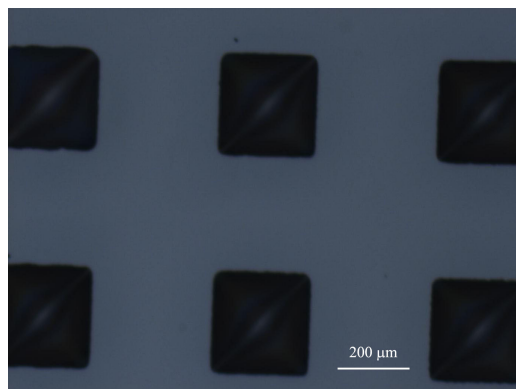
(a) DMSO droplets on a surface-energy patterned silicon wafer



(b) DMSO droplets on a surface-energy patterned glass substrate



(c) dodecane droplets on a surface-energy patterned glass substrate



(d) Glycol droplets on a surface-energy patterned glass substrate

Figure 4.7: Printing plates coated with various liquids by dip coating, showing the ability of selective wettability.

Printing plates can also be selectively coated with “inks” (solution containing materials to be printed) with dip-coating. Some of these examples are shown in Figure 4.8.

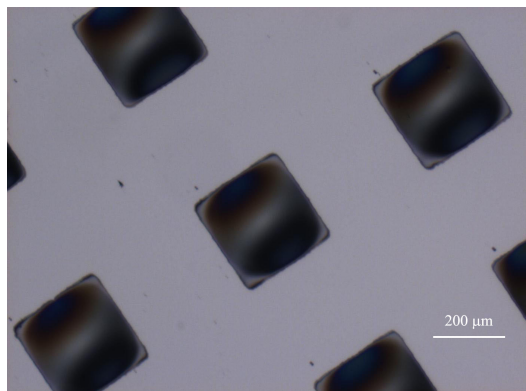
### 4.3 Printing Apparatus

In order to perform the printing work, a simple apparatus was constructed in the lab as part of this thesis. A schematic is shown in Figure 4.9a. The simple setup can perform basic functions required for a lab demonstration of the LAMP method. First, two vacuum stages are designed to hold the device plate and the printing plate in place. Second, in order to achieve alignment (both lateral registration and parallel alignment of the two plates), 6-way movement is required. A tilt and rotation stage and another XYZ stage are used for this purpose. A laser system is used for the parallel alignment, which contains a helium-neon laser, an aperture, a beam-splitter with adjustable holder, a lens and a screen. In addition, a CCD camera with a monitor is used for the visual inspection used for lateral alignment. Lastly, the whole setup is put under a fume hood with exhaust since toxic solvents are used. A photo showing part of the setup is given in Figure 4.9b.

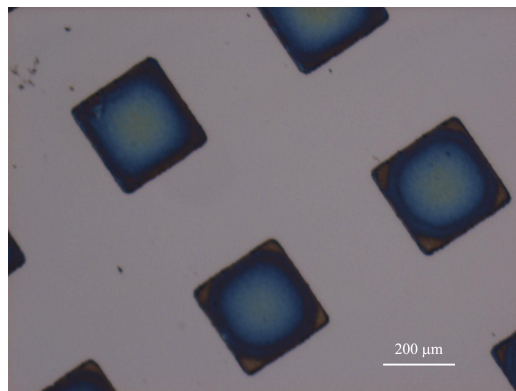
The parallel alignment of the two plates is of particular importance for successful demonstration of the LAMP method and is explained here in more detail. The laser alignment schematics used initially is shown in Figure 4.10a. For convenience, the incident and reflected laser beams are numbered and shown in different colors. Beam-0 is the incident beam which passes the aperture in the center of the screen. Beam-1 is the reflected beam from the top plate.<sup>2</sup> In our experiments, an ITO-coated glass substrate is used as the device plate and is put in this position. Because the glass plate

---

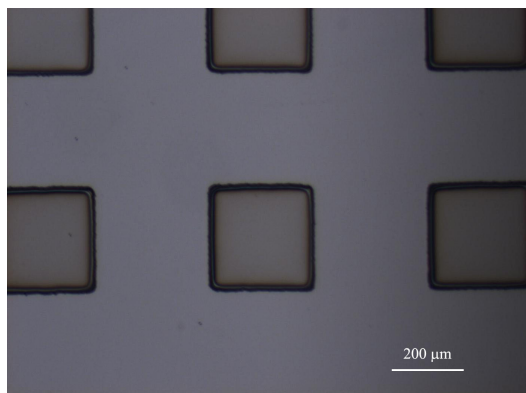
<sup>2</sup>In reality, two beams are reflected from the top plate, one from the top surface, one from the bottom surface. Since the top and bottom surface of the plate are almost perfectly parallel to each other and the beam is incident in a normal direction (after first step alignment), these two beams overlap with each other and are treated as one beam for simplicity.



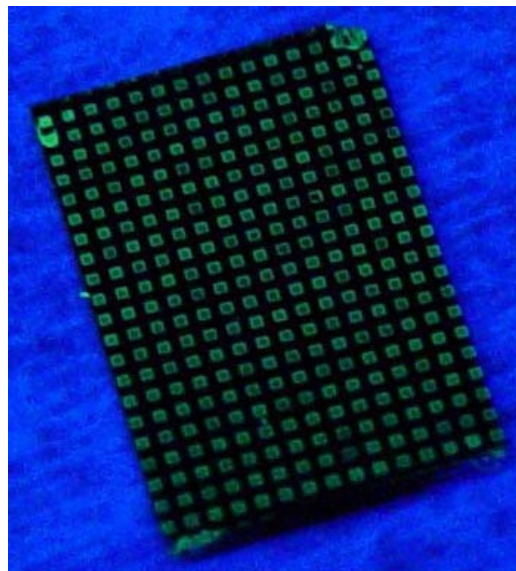
(a) Droplets of PEDOT:PSS in DMSO on a surface-energy patterned silicon wafer.



(b) After solvent evaporation, a thin layer of PEDOT:PSS is left.

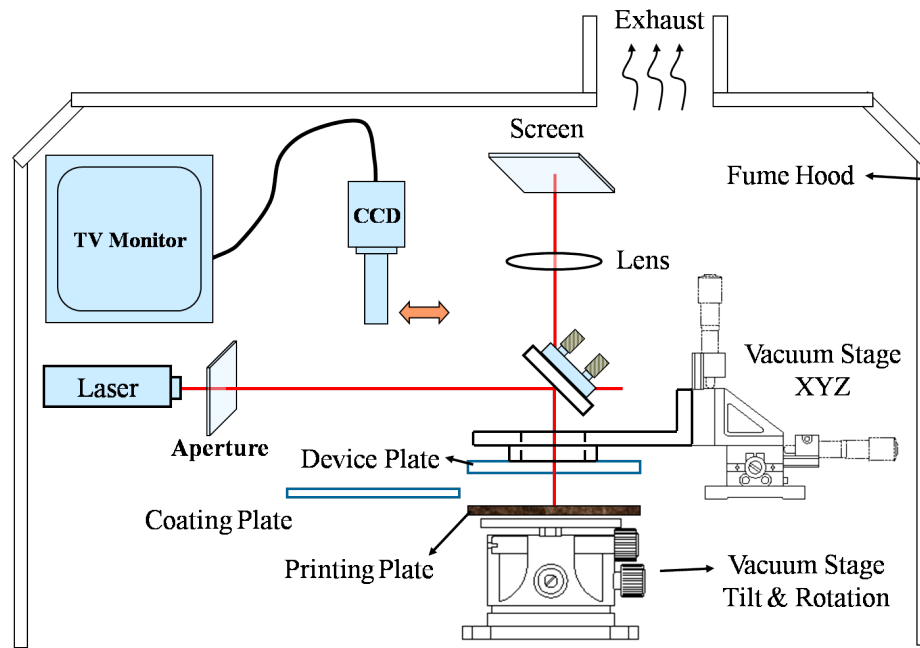


(c) PVK+PBD+C6 in dichlorobenzene droplets on a surface-energy patterned glass substrate.

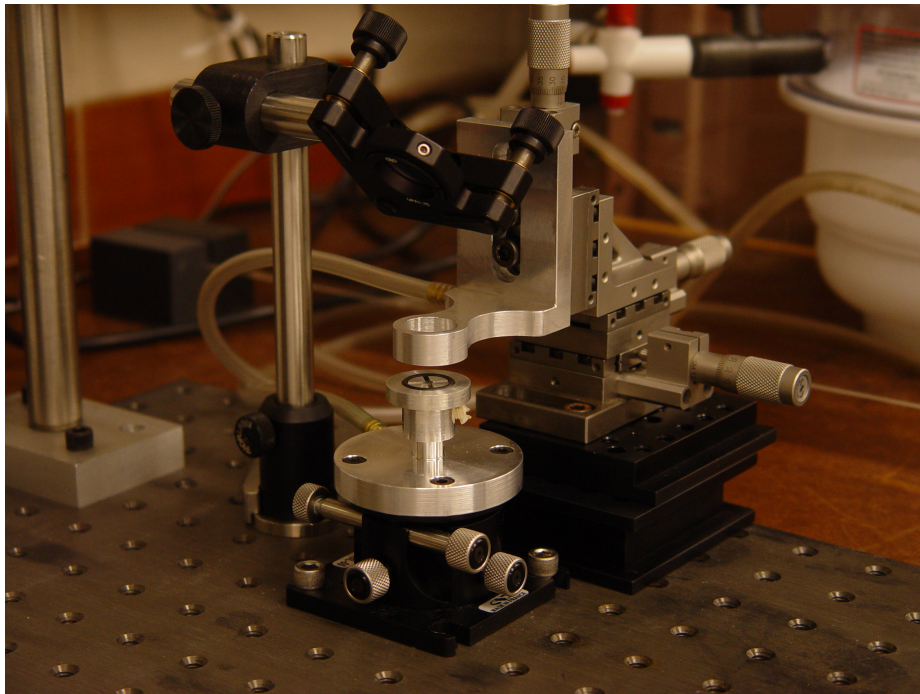


(d) After solvent evaporation, a thin layer of PVK+PBD+C6 is left. Photo taken with UV-photoluminescence.

Figure 4.8: Printing plates coated with organic solution (a, c) then allowed to dry, which resulted in a thin organic layer pattern (b, d).



(a) Schematic of the printing setup.



(b) Photo showing (from bottom up): bottom vacuum stage on a tilt and rotation stage, top vacuum stage on a XYZ stage, beam-splitter with adjustable holder, etc.

Figure 4.9: Lab setup used for the LAMP printing.

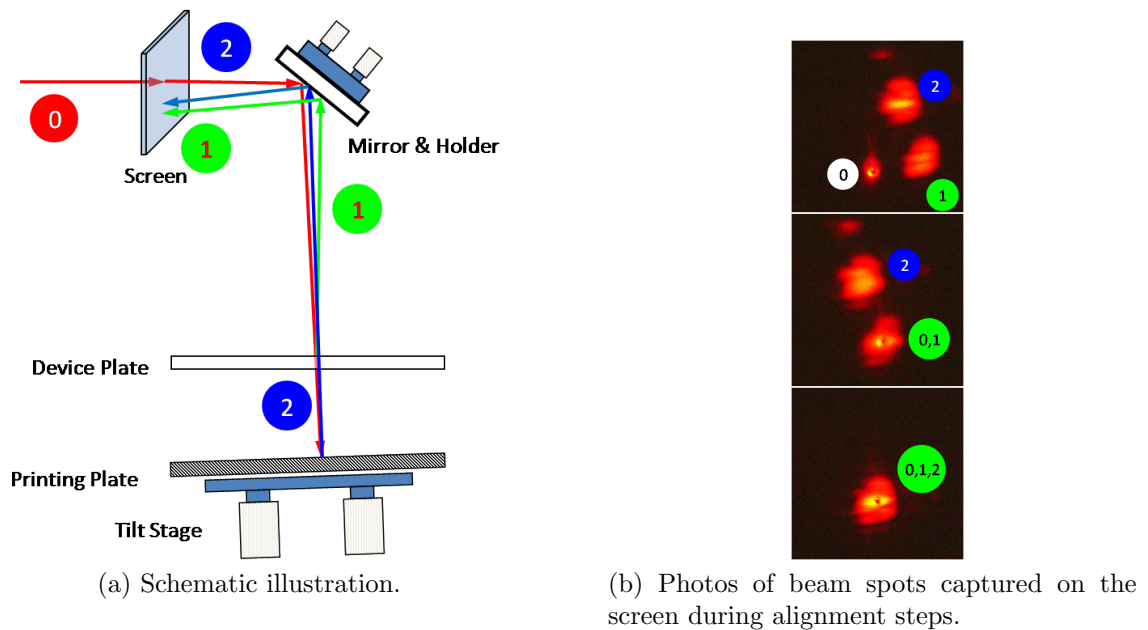


Figure 4.10: Schematics of laser alignment system.

is transparent the laser beam can transmit and reach the printing plate underneath. Beam-3 is the beam reflected from the printing plate surface, usually fabricated from a silicon wafer. Figure 4.10b shows three photos captured on the screen during the alignment steps. The top photo is taken when no alignment is done and thus different beams don't overlap. Alignment is achieved by first adjusting the orientation of the mirror (through the mirror holder) so that beam-1 overlaps with beam-0 (shown in the middle photo). This is to ensure that the laser beam-0 is now in normal incidence on the device plate surface. The next step of parallel alignment is to adjust the tilt stage underneath the printing plate so that beam-3 overlaps with beam-0 and beam-1 also (shown in the bottom photo). This step is to ensure that the printing plate is perpendicular to the incident laser beam-0. Now that both the top and bottom plates are perpendicular to the incident laser beam-0, these two plates are parallel to each other.

A simple calculation is utilized to estimate the accuracy of the parallel alignment illustrated in Figure 4.10.

$$\theta_{align} = \frac{\delta}{L} \approx \frac{1mm}{1.5m} = 6.7 \times 10^{-4} \text{radian} \approx 140 \text{arcsec} \quad (4.2)$$

$\theta_{align}$  refers to the alignment accuracy and  $\delta$  is the minimum overlap distance of the two laser spots.  $L$  is the distance between the screen and the printing plate. If we assume  $\delta = 1$  mm and  $L = 1.5$  m, the alignment accuracy is about 140 arcseconds. If the droplets are  $5 \mu\text{m}$  in height, this alignment accuracy is good enough to print droplets over a size range of about 7.5 mm.

A modified version of the laser alignment is shown in Figure 4.11. Here the laser beams reflected from the plates pass the beamsplitter and form a pattern on the screen located on the ceiling. A lens is used to magnify the pattern for better visual inspection. In this case, the incident beam is not present so the pattern is more clearly observed. This setup is similar to a Michelson interferometer and when the two plates are close to parallel, a pattern with stripes is formed. These are called Fizeau fringes or fringes of equal thickness. When the stripes become wider, the two plates are in better alignment, as illustrated on the right side of Figure 4.11.

The alignment accuracy can be estimated from the following equation:

$$\theta_{align} = \frac{\lambda}{2d} \quad (4.3)$$

$\lambda$  is the wavelength of the laser beam and  $d$  is the spacing between neighboring Fizeau fringes. For the helium-neon laser used,  $\lambda = 632.8\text{nm}$ . An example of the fringe pattern formed on the aperture screen is given in Figure 4.12. A square with a dimension of  $10 \text{ mm} \times 10 \text{ mm}$  was marked on the aperture screen. The two arrows mark the spacing of the center stripe, which is measured to be about 5.4 mm. Thus from Eqn. 4.3 the alignment accuracy is estimated to be about 12 arcseconds. By using this modified version of the laser alignment system, we are able to achieve a parallelism about an order of magnitude better than the first approach. This modified

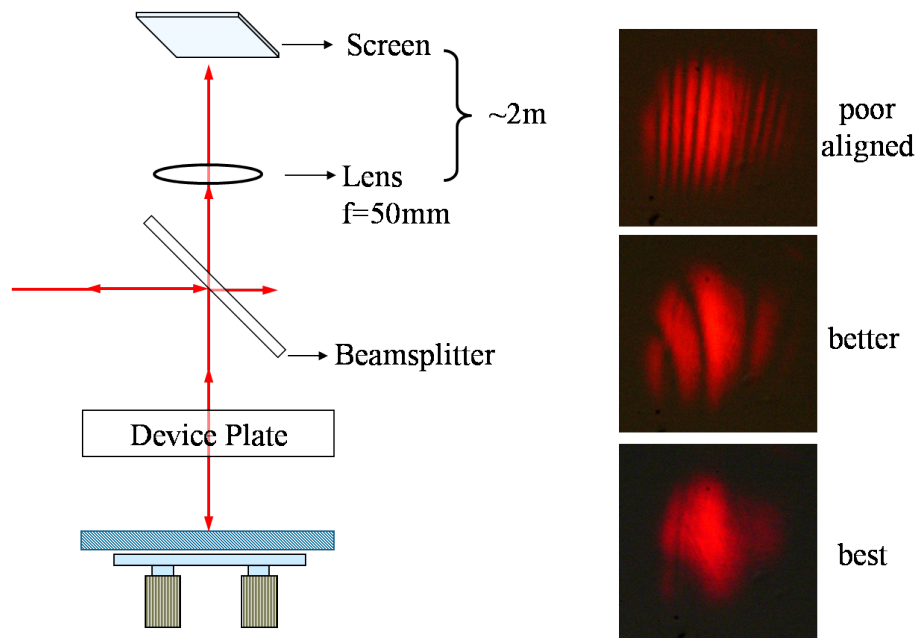


Figure 4.11: Improved laser alignment system with interference stripe patterns shown.

approach is the one illustrated in Figure 4.9a.

The tilt and rotation stage being used has a mechanical tilt sensitivity of  $\sim 2\text{--}3$  arcseconds. From our experience, by 3–4 times of the minimum turn of the tilt stage, a change in the fringe pattern is clearly visible, which agrees well with our previous calculation of the alignment accuracy.

In order to pattern RGB subpixel arrays, multi-step printing is required. Alignment marks are fabricated onto the printing and device plates for lateral alignment purposes.

## 4.4 Printing Experiments

### 4.4.1 Printing Procedure

In our experiments, the printing plate is coated with ink after the alignment is finished, so that it can be printed right after the coating before the inks dry on the printing plate. The printing plate can be coated with inks by dip coating. However, taking

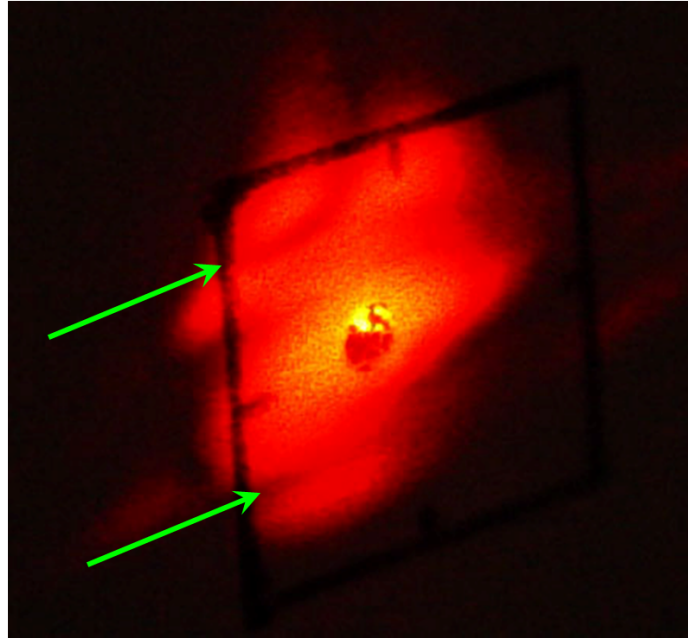


Figure 4.12: An example of the fringe pattern formed on the aperture screen, taken when the alignment is close to best. The black square on the screen has a dimension of  $10\text{ mm} \times 10\text{ mm}$ . The center stripe has a spacing of about  $5.4\text{ mm}$ , illustrated by the two arrows. The alignment accuracy is estimated to be about  $12\text{ arcseconds}$ .

the printing plate out for dip coating and putting it back to the tilt stage will require re-alignment. Instead of dip coating, a meniscus coating method is applied in our experiments. In meniscus coating, another coating plate wetted with ink is brought into contact with the printing plate and is slowly pulled, sliding over the printing plate surface. As a result, the printing plate surface will be selectively coated with inks, depending on the surface wettability pattern.

Once the alignment and coating of the printing plate is finished, the top (device) plate is lowered into contact with the bottom (printing) plate by operating the XYZ stage. The CCD camera monitoring system is switched in after the alignment is done, which is used to monitor the spacing between the two plates. In the experiments, the spacing is not precisely controlled. Rather, the top plate is lowered until droplets on the bottom plate are in contact with the top plate. Care is taken to prevent neighboring droplets from touching each other when pushed too much.

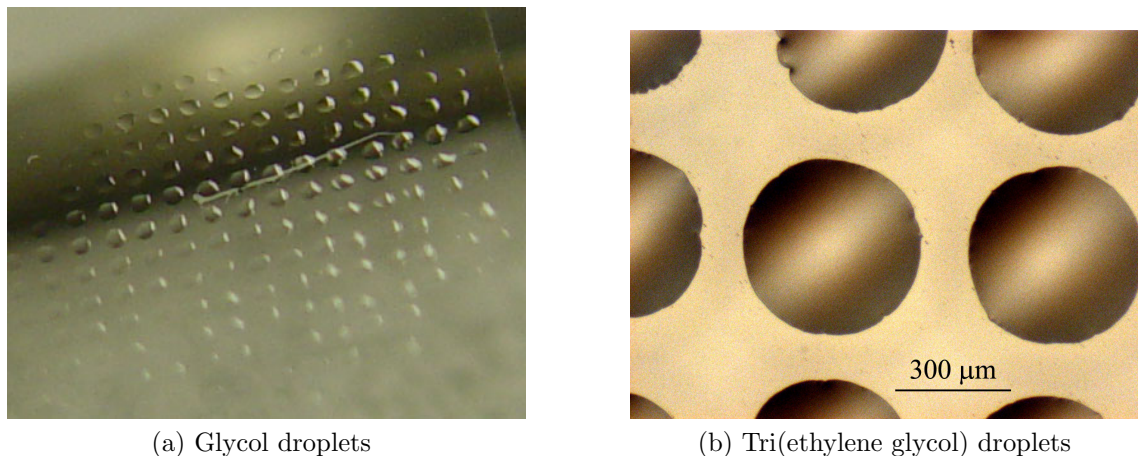


Figure 4.13: Solvent droplets printed onto glass substrates as demonstrations of the LAMP method. Droplets have a spacing of  $600\mu m$  for both images.

#### 4.4.2 Printing Solvents

As a first demonstration, low-evaporation-rate solvents were being printed. A low evaporation rate is important, so that the solvent does not dry on the printing plate before the printing process. Figure 4.13 shows photos of printed droplets on a glass substrate by LAMP method. Glycol and tri(ethylene glycol) droplets are successfully printed onto glass substrates with a spacing of  $600\mu m$  between neighboring droplets, which is defined by the surface energy pattern of the printing plate.

#### 4.4.3 Printing Small Molecules

As discussed in Chapter 3, chlorobenzene is often used as the solvent for our PVK + PBD + dye mixture. However, chlorobenzene has a very high evaporation rate. In our experiments, the droplets are about  $300\mu m$  in diameter and they disappear in several seconds. We do believe that this amount of time is enough for automated high speed printing (as in the newspaper printing, for example), but it is too short, however, to allow us enough time to print manually.

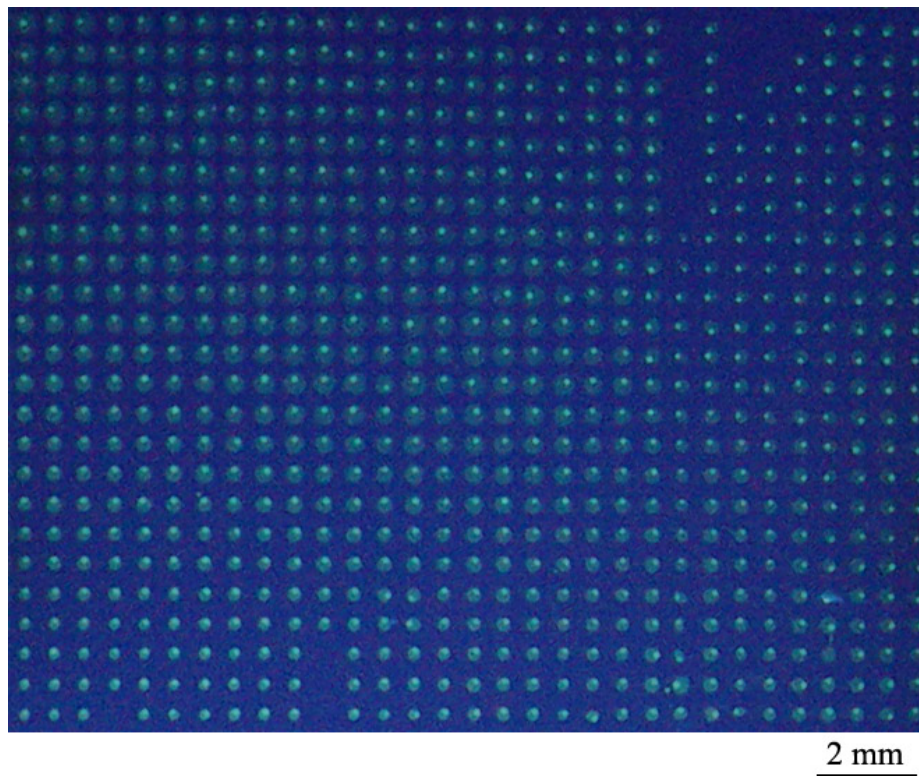
In contrast to PVK which only dissolves in selective solvents, small molecules can more easily dissolve in a wider range of solvents, and thus are easier to work

with. While polymers are more difficult to pattern, an alternative way for OLED color patterning is to deposit and pattern three kinds of dyes used for RGB colors, respectively, onto a host polymer. The patterning of small molecular dyes has been demonstrated earlier in our group by either an ink-jet printing method [25] or a dye diffusion method [54, 55].

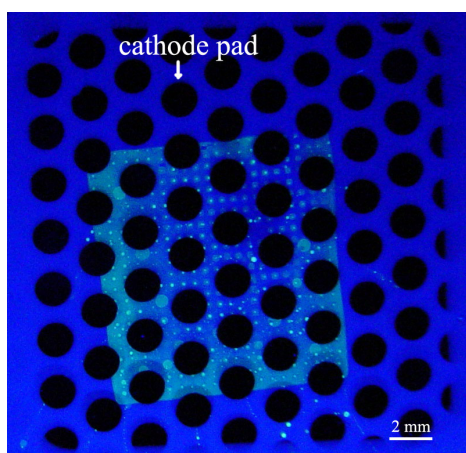
In a similar way, we demonstrated that the LAMP method can be utilized to print small molecular dyes for color OLED patterning. In our experiments, we first spin coat a PVK+PBD layer on a glass substrate. Then, C6 used for green light emission is printed onto the polymer layer. DMSO is a solvent with slow evaporation rate and C6 is dissolved into DMSO to form a solution (0.02 mg/ml). The printed results are shown in Figure 4.14a. The printed pixels have a nominal diameter of  $300\mu m$  with a spacing of  $600\mu m$ . A Mg:Ag cathode layer is evaporated on top of the PVK+PBD and printed C6 layer to make OLEDs. Figure 4.14b is a UV photoluminescent image of the fabricated devices. I-V curves of the printed devices with comparison to spin-coated control devices are shown on Figure 4.14c. The I-V curves show that the printed devices perform well without any optimization of the printing. Note also that the cathode has a diameter of about 1.6 mm and the printed droplets are only  $300\mu m$  in diameter. So in the printed devices, not all area contains C6, which contributes to a lower efficiency. In contrast, in the spin-coated devices C6 is premixed into the solution and is homogenous in the film.

#### 4.4.4 Printing Polymers

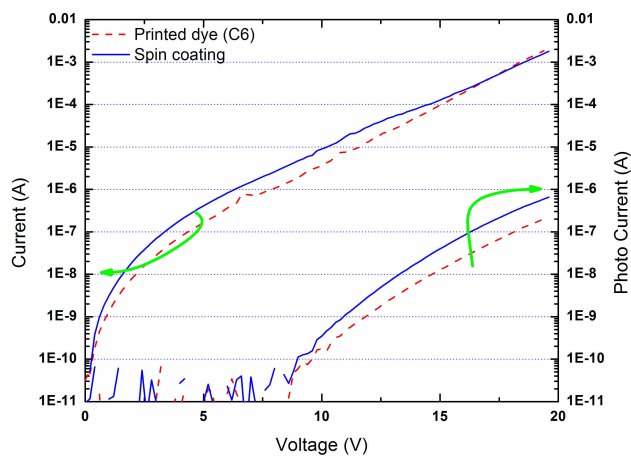
In order to print PVK (or the mixture PVK+PBD+dye) we needed to find a solvent that is able to dissolve PVK while having slow evaporation rate to allow enough time for printing. We found that 1,2,4-trichlorobenzene (hereafter trichlorobenzene) can successfully dissolve PVK, and the droplet can withstand about 1 minute before drying, which is long enough to finish our printing. Thus, trichlorobenzene has been



(a) UV photoluminescence image showing green dye (C6) array printed on top of a PVK+PBD layer.

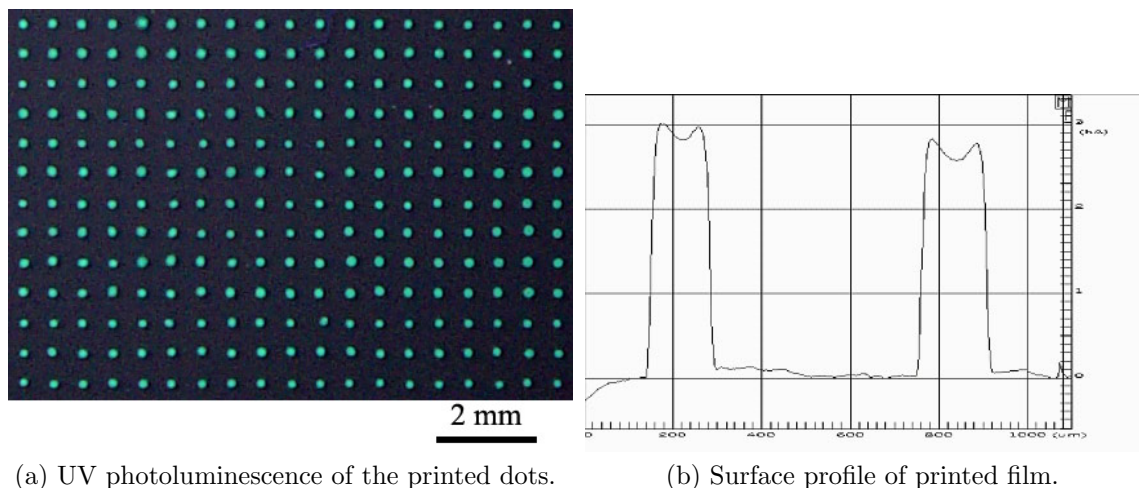


(b) UV photoluminescence image of the printed array after cathode evaporation.



(c) I-V curves of OLEDs with printed C6 in comparison with regular spin-coated devices.

Figure 4.14: Small molecular dye (C6) printed onto a glass substrate pre-coated with a PVK+PBD layer. Spacing between pixels are  $600\mu\text{m}$ .



(a) UV photoluminescence of the printed dots.

(b) Surface profile of printed film.

Figure 4.15: PVK+PBD+C6 in trichlorobenzene printed onto a glass substrate.

utilized as the solvent to print the mixture PVK+PBD+dye in our work.

As will be discussed later in Section 4.5, however, OLED devices printed with trichlorobenzene did not work. We switched back to chlorobenzene again as the solvent for printing PVK+PBD+dye mixtures. A solvent-vapor-saturated closed system was utilized to extend the droplet lifetime before evaporation, which made the printing possible. In this section, however, printing results with trichlorobenzene solvent will be shown.

### Droplet Un-constrained Printing

Figure 4.15 shows the printing results of a PVK+PBD+C6 green mixture with trichlorobenzene solvent on a un-patterned flat glass substrate. Figure 4.15a is a photo of the printed array under UV illumination. The printed pixels have a spacing of  $600\mu\text{m}$  and a typical surface profile scan of the printed film is shown in Figure 4.15b. Notice that due to the unpinning of the droplet contact lines, the dried film diameter is smaller in size than original droplet (diameter of  $300\mu\text{m}$ ).

In real devices, light-emitting inks are often printed onto wells formed with insulating banks. The banks of the wells act as the insulating layer between the two electrodes which would otherwise make short contacts. In our experiments, a  $\text{SiN}_x$

layer on top of the ITO layer is used as the insulating layer and wells are made onto the  $\text{SiN}_x$  layer by photolithography followed with RIE etching. As shown on Figure 4.16a, droplets of PVK+PBD+C6 in trichlorobenzene can then be printed onto the wells. The diameter of the openings is  $300\mu\text{m}$  with a spacing of  $600\mu\text{m}$ . Figure 4.16b is a UV photoluminescence image of the printed array, Figure 4.16c is an optical micrograph of a typical pixel, Figure 4.16d is a typical surface profile scan of the printed layer on the well. Notice that since the printed droplets are not confined, the droplets smear out and cover more area than the openings of the  $\text{SiN}_x$  layer. More material is deposited on the edge of the pixel, due to the “coffee-ring” effect [18]. The spreading of the droplets will cause material breaching into neighboring subpixels for a different color emission and needs to be prevented. In addition, the material built up around the edge is bad for uniform light emission.

### **Droplet-Constrained Printing**

In order to better confine the position of printed droplets, the device plate can be surface-energy treated before the printing [58]. As shown in the schematic of Figure 4.17a, the same PFOTS self-assembly layer has been grown on the surface of the  $\text{SiN}_x$  layer to prevent undesired droplet wetting. Due to the presence of the PFOTS layer, the printed droplets are well confined within the wells. This is shown in the improved pixel shapes after the evaporation of solvents, as shown in the UV photoluminescent image of Figure 4.17b. The surface profile of a typical printed pixel given in Figure 4.17c also shows that all material is deposited within the well.

### **Printed RGB Arrays**

So far we have only printed single-color arrays of light-emitting materials by the LAMP method. Our goal is to show that LAMP is capable of patterning R, G, B sub-pixel arrays required for a full-color display. Three-color printing is straightforward,

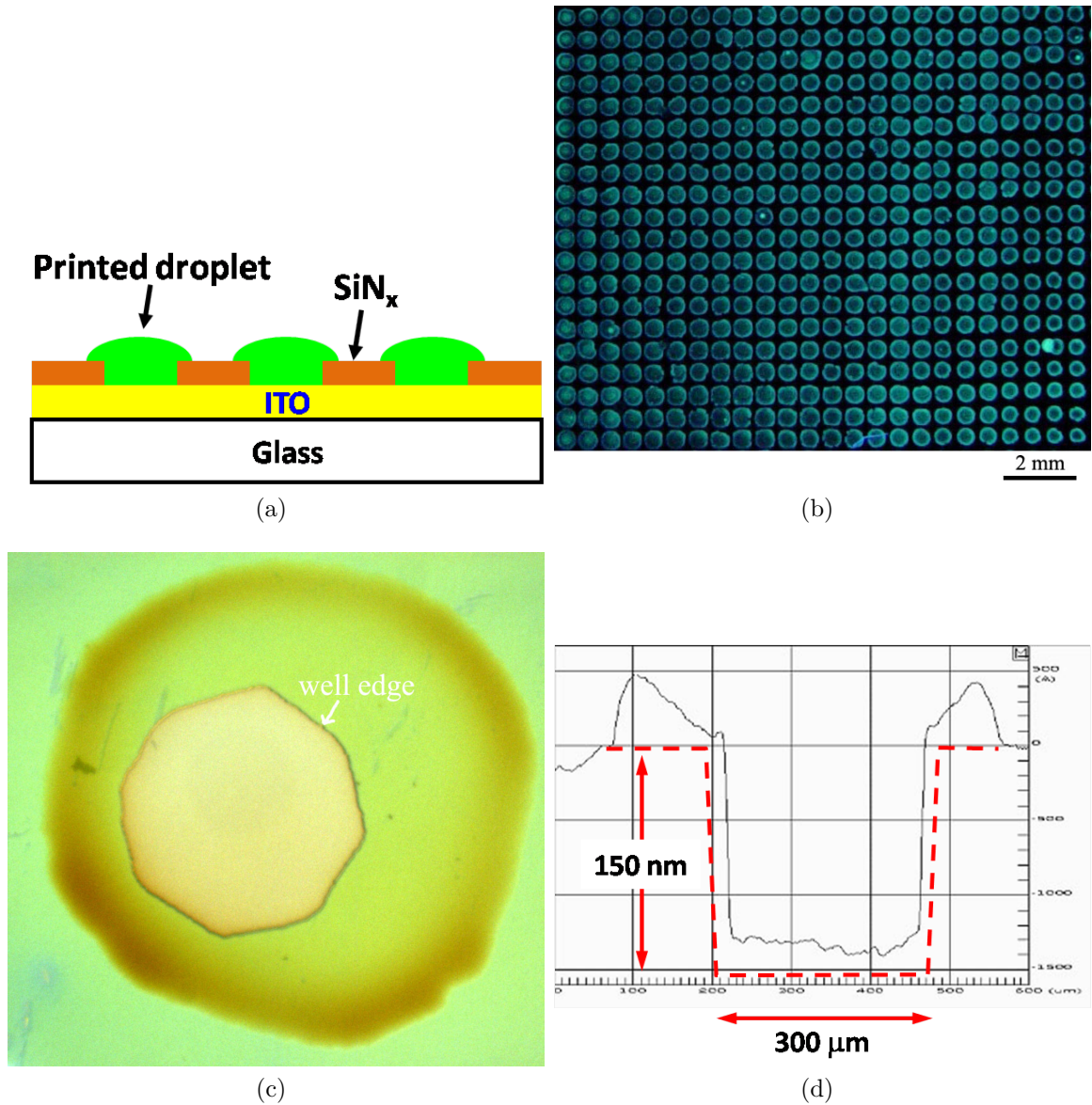


Figure 4.16: Printed green mixture with trichlorobenzene onto a SiN<sub>x</sub> patterned glass substrate. (a) Schematics of the printing, (b) UV photoluminescent image of the printed array, (c) an optical micrograph of a typical printed pixel, (d) a typical surface profile scan of the printed layer (dashed line is the outline of the well).

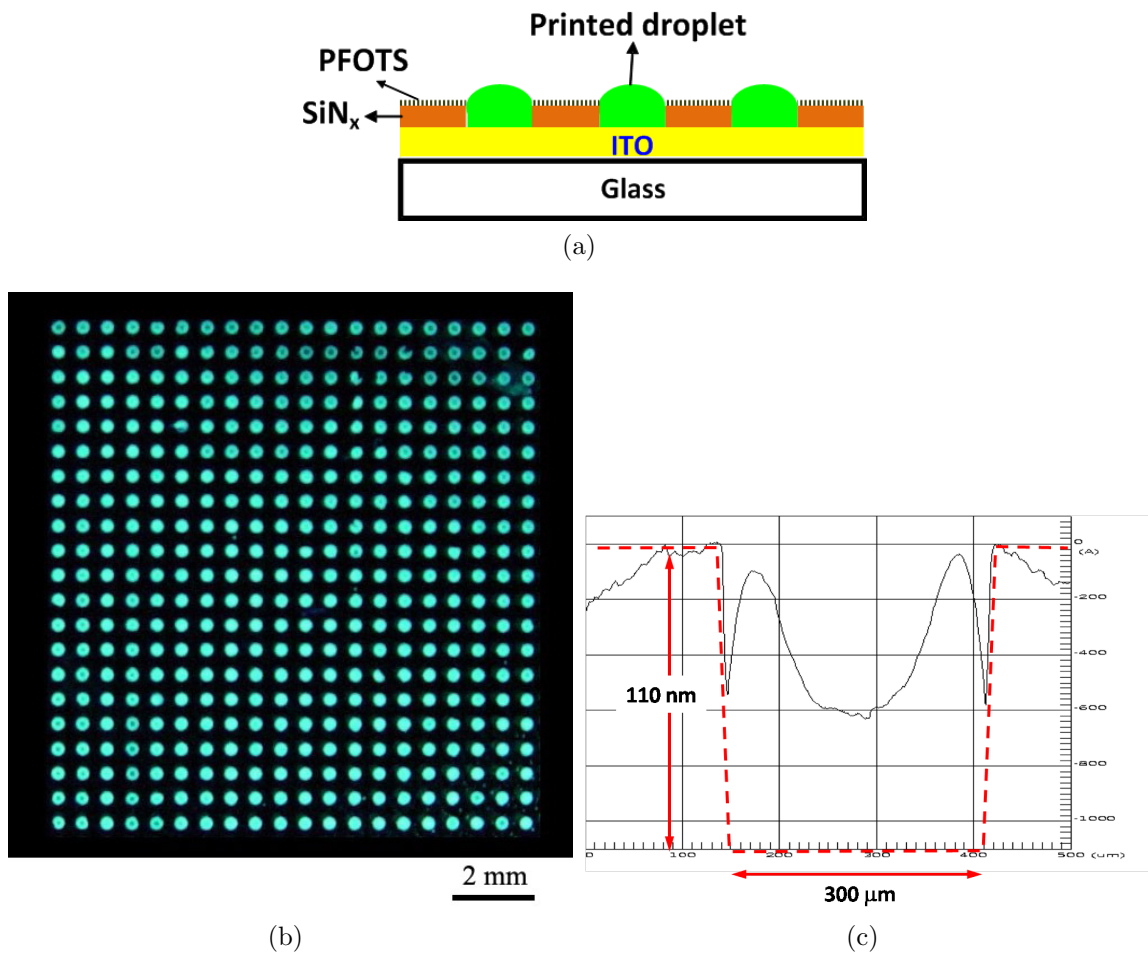


Figure 4.17: Printing onto a droplet constrained substrate. (a) Schematics, (b) UV photoluminescence of the printed arrays showing improved uniformity of pixel dimensions due to the confinement of droplets on the substrate. (c) A typical surface profile scan of the printed film (dashed line is the outline of the well).

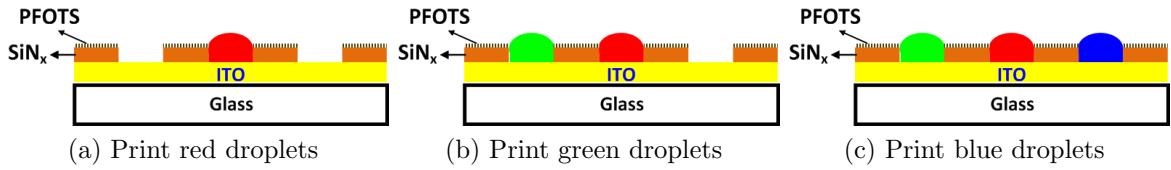


Figure 4.18: Schematics for the printing of RGB arrays.

however, once single-color arrays can be printed. Figure 4.18 shows the procedures used for printing RGB arrays. Printing results are shown in Figure 4.19.<sup>3</sup> Figure 4.19a is a UV photoluminescence photo taken after the first step of printing (red pixels) and Figure 4.19b is after the printing of green pixels and Figure 4.19c is after the printing of blue pixels. Since these RGB arrays are the main results of our LAMP method demonstration, an additional printed RGB arrays is shown as Figure 4.19d.

As can be seen from Figure 4.19, although there are several pixels missing as a result of the simplicity of the printing apparatus, it is clear that the LAMP method is capable for organic layer patterning for full-color OLED applications. In addition, since the LAMP process is a parallel process, so the throughput could be high compared to serial process utilized in ink-jet printing. We believe that this method is of low-cost potential, especially if roll-to-roll processing were to be utilized.

## 4.5 Device Performance and Solvent Revisited

Since active layers are being deposited and patterned in this work, their electrical and optoelectronic properties need to be investigated for successful demonstration. We therefore carried out electroluminescence experiments to study the performance of devices containing our printed layers. From a series of experiments, we have found out that devices prepared with trichlorobenzene are extremely resistive and do not emit light. Some of the results have been summarized on Figure 4.20. OLEDs are

<sup>3</sup>Note that the colors shown in Figure 4.19a, b and c are off due to the difficulty to achieve accurate white balance of the digital camera under UV light. The colors in Figure 4.19d have been manually tuned to reflect a more accurate color perceived by human eyes.

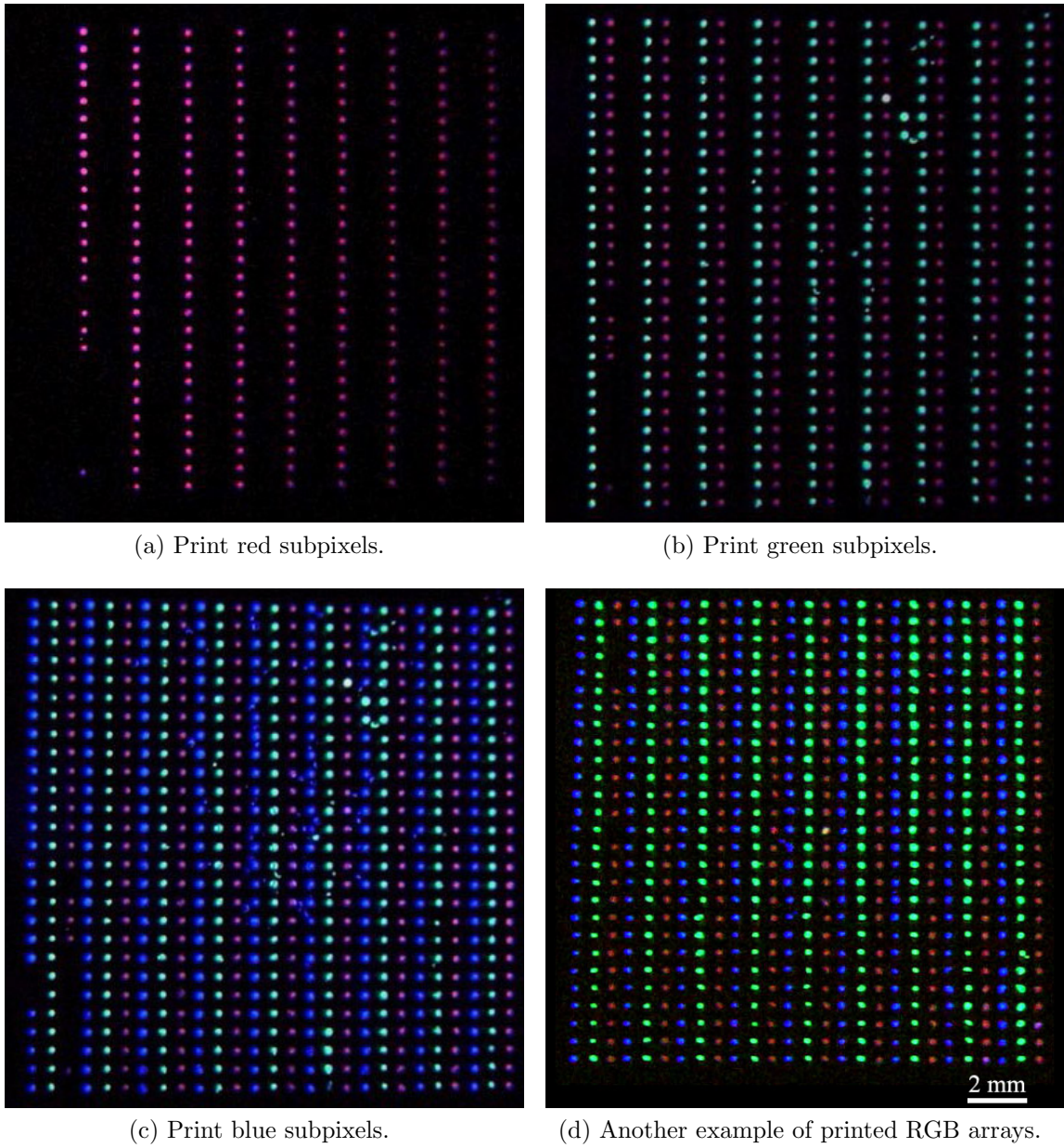


Figure 4.19: RGB arrays formed by three successive steps.

fabricated following the general recipes outlined in Chapter 3, except that different approaches were used to prepare the light-emitting layers (PVK+PBD+C6 in a mixture). In Figure 4.20a the green mixture is spin-coated from chlorobenzene solvent. Devices made in this way are used as the control devices. In Figure 4.20b, the green-emitting mixture is spin-coated from trichlorobenzene solvent. These devices show no light emission (measured photocurrent within noise/stray light level) and the device current is low ( $\sim 1 - 10 \mu A$  at 25 Volt). Since trichlorobenzene is a solvent with high boiling temperature and slow evaporation rate, we expect that solvent residue may exist in the prepared devices which caused the low current injection. Thus, various baking approaches have also been explored to try to remove trichlorobenzene residue, such as (1) baking at  $70^\circ C$  for 15 minutes in a glove box after the spin-coating, (2) baking at  $100^\circ C$  for 20 minutes in a nitrogen glove box after the spin-coating, and (3) keeping the spin-coated layer under a vacuum of  $10^{-6}$  Torr for 20 hour, etc. All these baking approaches yielded no noticeable improvement on the device performances. In Figure 4.20c the green-emitting mixture layer was printed by LAMP method followed by a baking at  $100^\circ C$  for 20 minutes in a nitrogen glove box. In Figure 4.20d, the ITO/glass substrate is first spin-coated with trichlorobenzene solvent (without any solute) followed by a baking at  $100^\circ C$  for 10 minutes in a glove box to remove any solvent residue. The green mixture was then deposited the same way as the control device of Figure 4.20a. Poor performance was again observed, as shown in Figure 4.20d. The I-V curves shown in Figure 4.20, especially the results of Figure 4.20d reveal that trichlorobenzene residue may exist at devices involving trichlorobenzene solvent during processing, and the residue has an unknown deleterious effect on devices.

### 4.5.1 Modified Printing Setup

After extensive experiments with trichlorobenzene as the solvent, which all failed electroluminescent tests, we decided to switch back to the fast evaporating solvent:

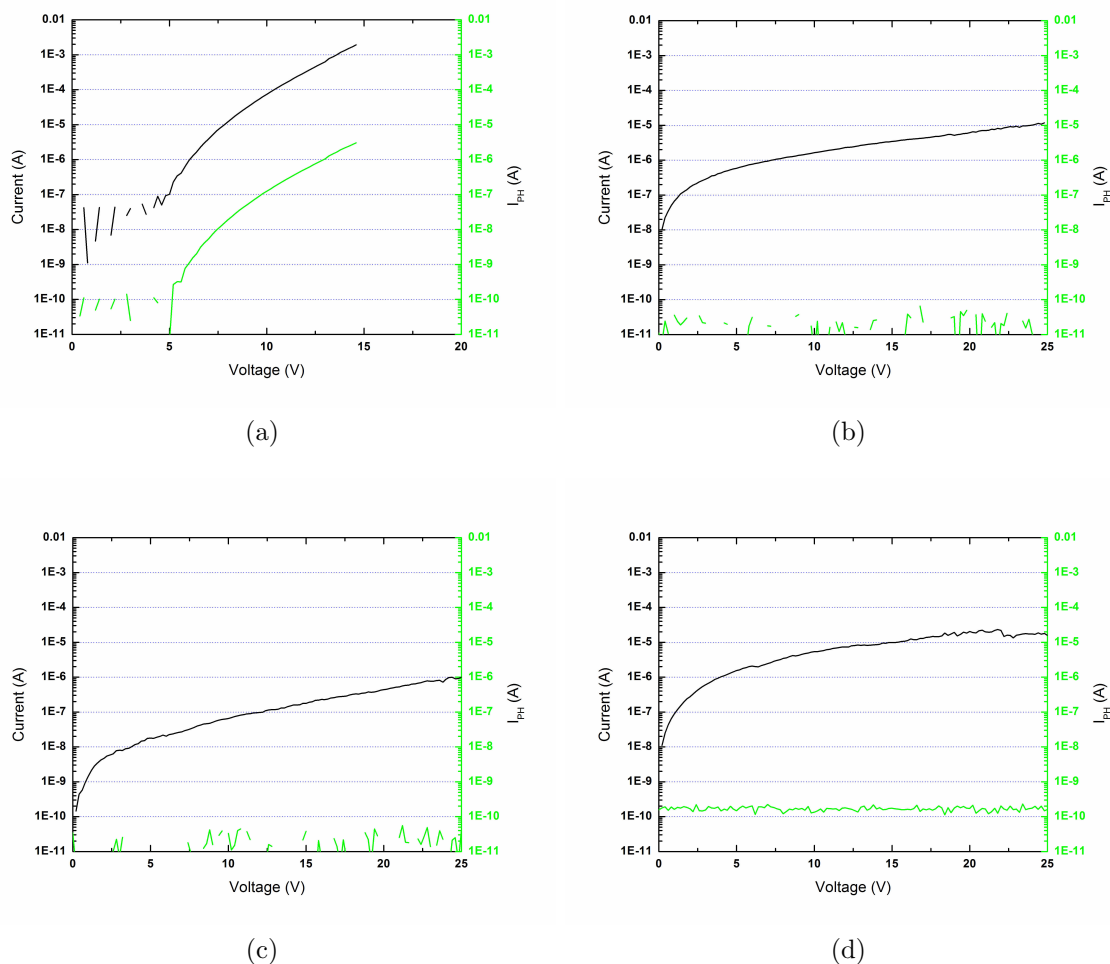


Figure 4.20: Effect of trichlorobenzene solvent on device I-V curves. Curves shown here are typical curves of device current and detected photocurrent vs applied voltage measured on devices containing the green-emitting mixture PVK+PBD+C6 deposited by various methods: (a) spin coating of green mixture in chlorobenzene solvent (control device), (b) spin coating of green-emitting mixture in trichlorobenzene, (c) green-emitting mixture in trichlorobenzene printed by LAMP method, (d) spin coat trichlorobenzene solvent followed by baking, then spin coating of green-emitting mixture in chlorobenzene solvent.

chlorobenzene. Note that we first resorted to the use of trichlorobenzene as the solvent because it will allow us enough time for the printing. In order to work with chlorobenzene, however, other approaches need to be taken in order to extend the droplet lifetime for printing. We then utilized the idea of a closed system with saturated-solvent-vapor environment to extend the working time for printing. Such a closed system, however, may not be necessary for an automated printing system since printing could be made very fast, like how newspapers are printed today.

In order to print within a closed system, we basically need to put our printing setup into a glove box, with extra chlorobenzene solvent to achieve a saturated vapor environment. Due to lab limitations, we have utilized a simple glove bag for our closed system printing demonstration. Figure 4.21a shows an illustration of the glove bag. We are able to put the two vacuum stages, the XYZ-stage and the tilt-and-rotation stage inside the glove bag, together with a glass dish with plenty of chlorobenzene. Other parts of the printing setup shown in Figure 4.9 are left outside the glove bag. Laser alignment is achieved with laser beams pass through the thin plastic film of the bag. With this glove bag printing system, light-emitting layers can now be printed with chlorobenzene solvents and a typical printed arrays are shown in Figure 4.21b. As a result of the simplicity of the printing apparatus and difficulties in operation, the printed results are not as good as our printing results with trichlorobenzene shown in Figure 4.17.

### 4.5.2 Device Measurement

In order to study the effect of printing on device performance with chlorobenzene solvent, OLEDs with the green mixture as the light-emitting layer are fabricated. Devices begin with ITO-coated glasses. A  $\text{SiN}_x$  layer is deposited onto the ITO layer, acting as the insulating layer between cathode and anode. Small openings on the  $\text{SiN}_x$  layer with diameter of  $300 \mu\text{m}$  and a spacing of  $600 \mu\text{m}$  (a fill factor of about

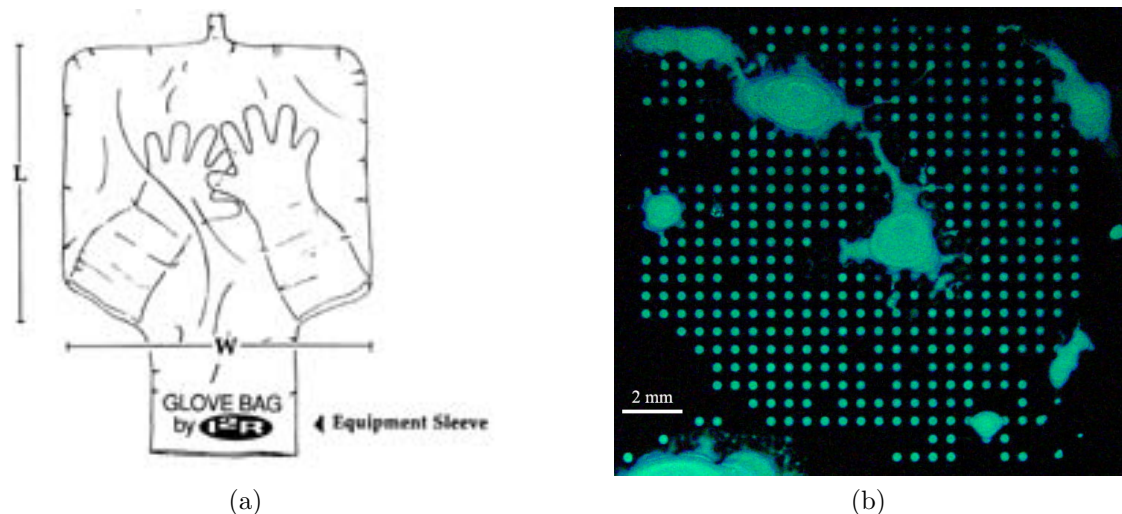
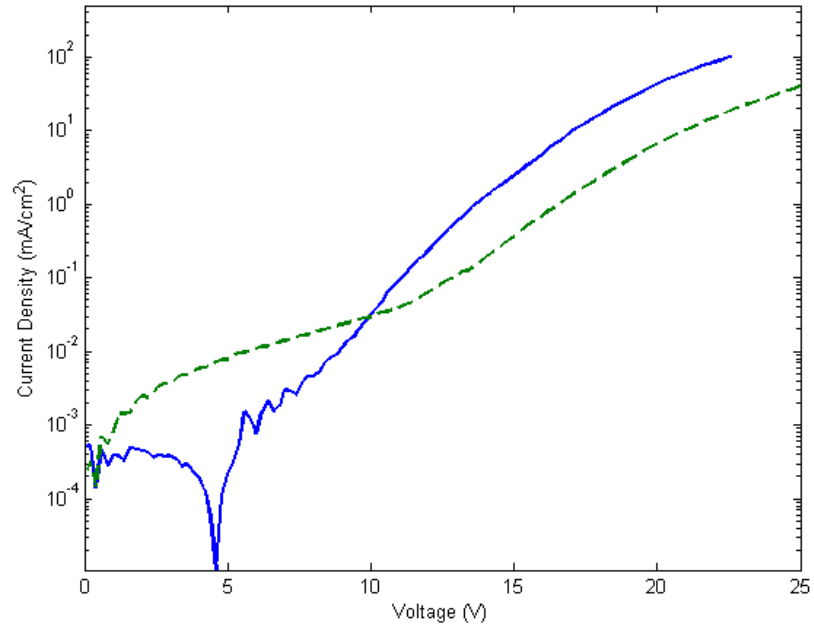
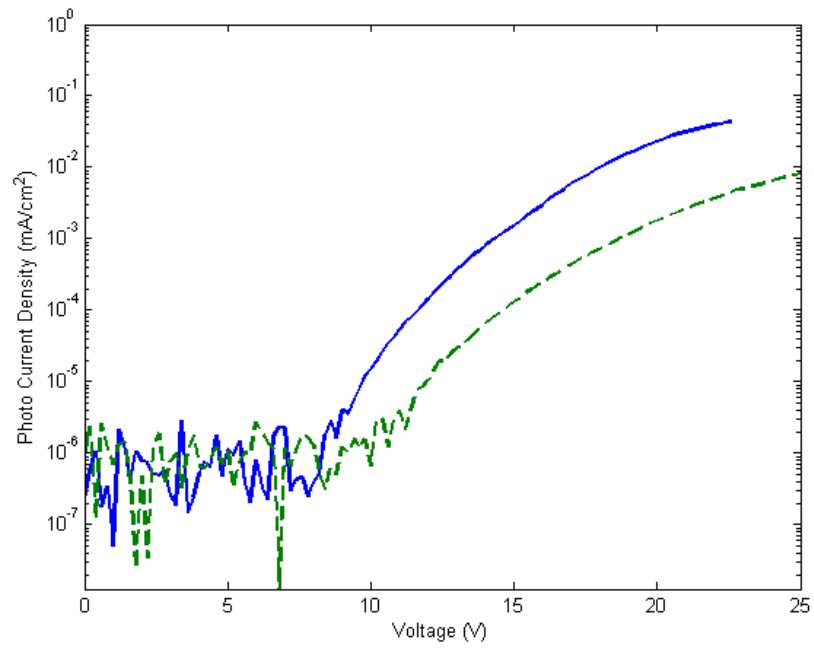


Figure 4.21: LAMP printing achieved with chlorobenzene solvent within a vapor saturated close system. (a) A plastic glove bag is used to form a closed system. Printing is done within the glove bag where the atmosphere has been saturated with chlorobenzene solvent vapor to extend the lifetime of droplets to allow enough time for printing. (b) Printing results of green pixels with chlorobenzene as solvent within the glove bag.

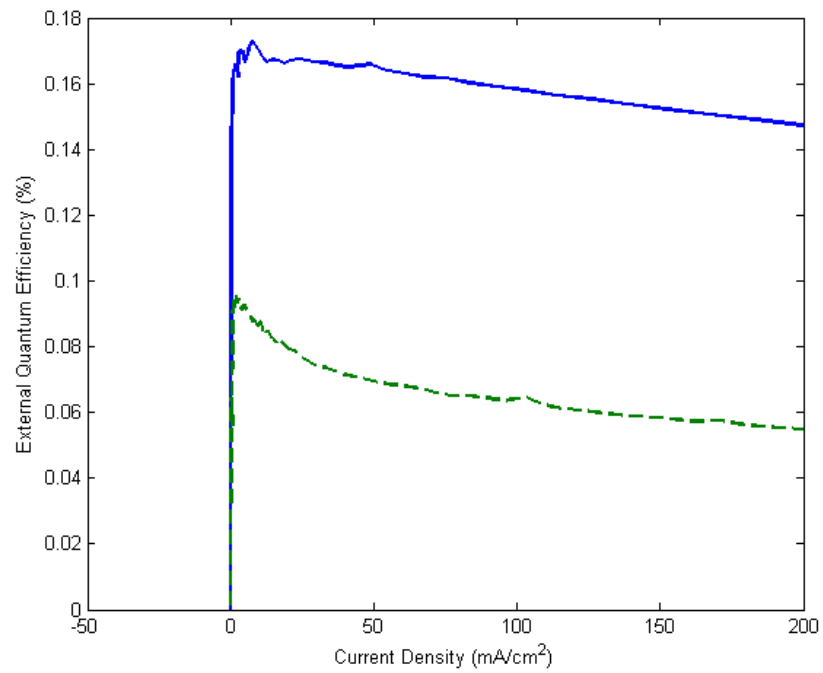
0.196) were made by photolithography followed by RIE etching, which defines the OLED pixels. The light emitting layer is then deposited onto the small pixels with exposed ITO surface from chlorobenzene solvent. After the drying of droplets, a Mg:Ag cathode is deposited on top of the organic layer to finish the device. The cathode area is defined by the shadow mask and has an area of  $2 \text{ mm}^2$ . Since each cathode pad of  $2 \text{ mm}^2$  covers several small pixels, the actual average area of the OLED being tested is estimated (with a fill factor of 0.2) to be  $0.4 \text{ mm}^2$ . Control devices are made the same way, except that the light-emitting layer is deposited by spin-coating, rather than printing. I-V curves of these devices are shown in Figure 4.21. The maximum external quantum efficiencies of the printed devices are roughly half the value of the spin-coated controls, as shown in Figure 4.21c. This number is quite good, taking in account that the printed layer thickness and profile uniformity has not been optimized and the extra time of exposure to air during printing, etc.



(a)



(b)



(c)

Figure 4.21: I-V curves of OLEDs with organic layer deposited by spin-coating (solid line) or printing (dash line) with chlorobenzene solvent. (a) OLED injection current (b) OLED photo current (c) Calculated external quantum efficiency.

### 4.5.3 Passive Matrix Display

For a better demonstration, a small passive matrix display was fabricated and tested. Five masks for photolithography were designed for the patterning of: ITO anode stripes, Au connection pad,  $\text{SiN}_x$  layer opening, PFOTS self-assembly on  $\text{SiN}_x$  layer, and the printing plate. An additional shadow mask was designed for the thermal deposition of the cathode layer. The OLED structure used here is the same as earlier, except that an additional 80-nm  $\text{Alq}_3$  layer is thermally evaporated on top of the regular light-emitting layer to reduce the leakage current of the OLED pixel under reverse voltage [48]. An in-house setup for the testing of passive matrix displays was built up by a former graduate student in our group, Ke Long [48]. A printed circuit board was also designed, which connects the display to Ke's setup. The setup is driven by a computer with a custom LabVIEW program. Figure 4.22 shows the image of a passive display (by spin coating) under test, with the printed circuit board underneath.

By changing the setting in our LabVIEW program, we can drive the passive matrix display so as to show some patterns. For example, Figure 4.23 shows a  $6 \times 12$  display made by spin-coating showing three different patterns.

A passive matrix OLED display with the green light-emitting layer deposited by the LAMP method is also shown on Figure 4.24. Figure 4.24a is an optical micrograph of the display after the deposition of the PVK+PBD+C6 layer. Figure 4.24b shows a  $4 \times 7$  array under test. This demonstrates the ability of our LAMP method for OLED display fabrication. Notice that the light-emission of the printed display is not uniform, compared to the spin-coated displays, which we believe is a result of non-uniform film thickness of the printed films after drying. This issue will be further discussed in Chapter 5.

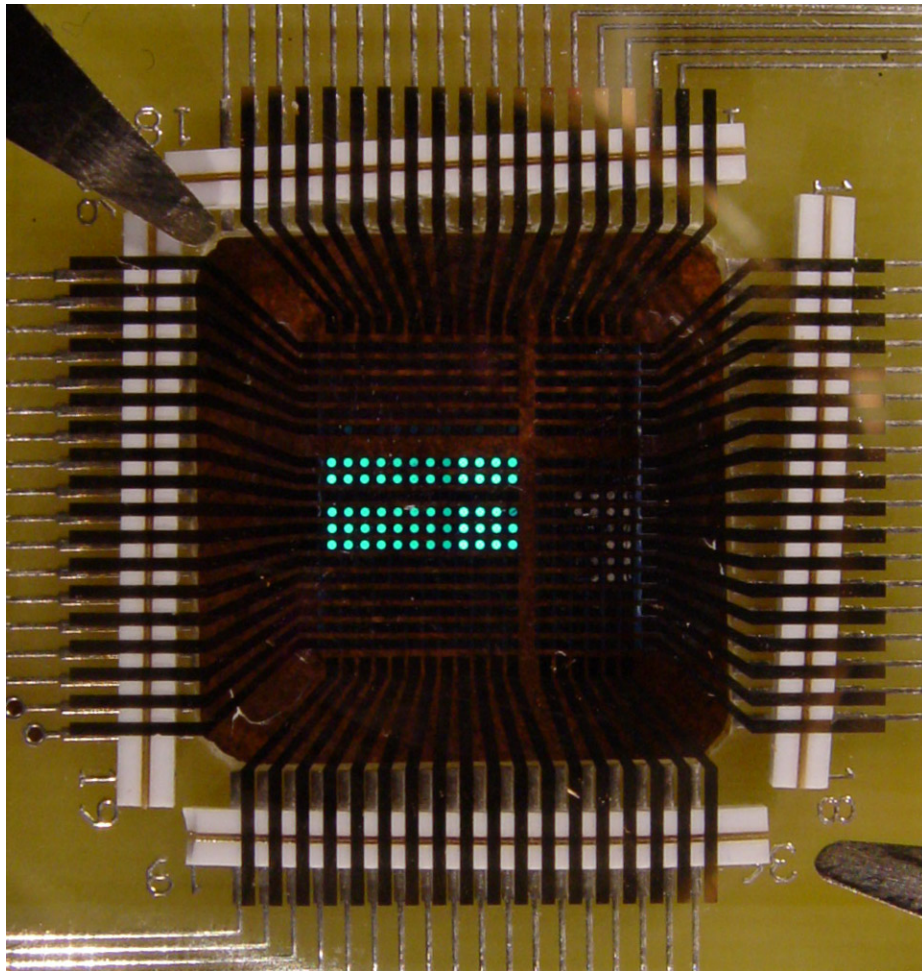


Figure 4.22: A passive matrix display (by spin coating) under test. The printed circuit board is also shown. 6 rows  $\times$  12 columns of pixels are driven. The third row is missing, probably caused by a shorted pixel.

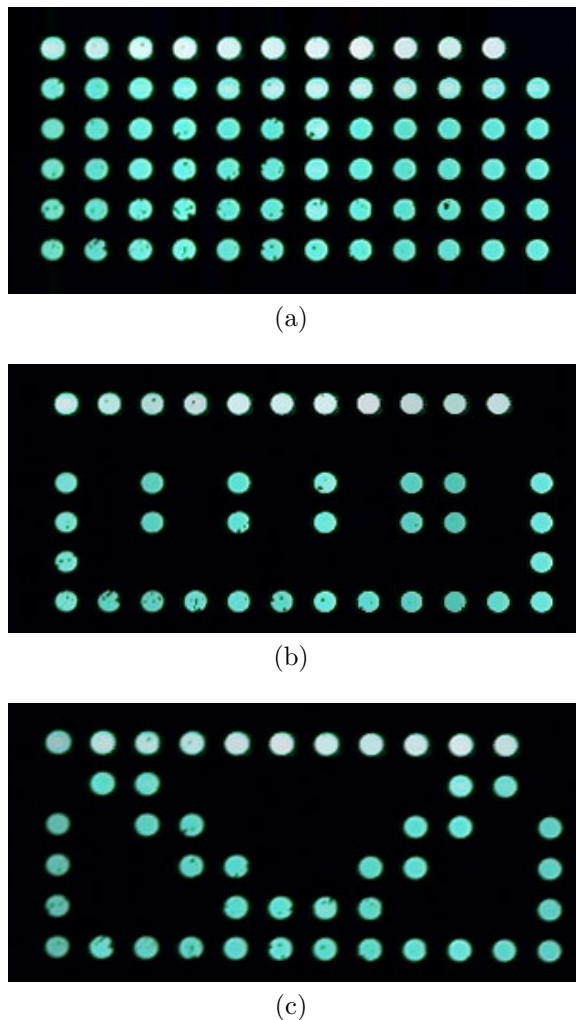


Figure 4.23: A passive matrix OLED display, with the light-emitting layer spin-coated, is driven with three different patterns.

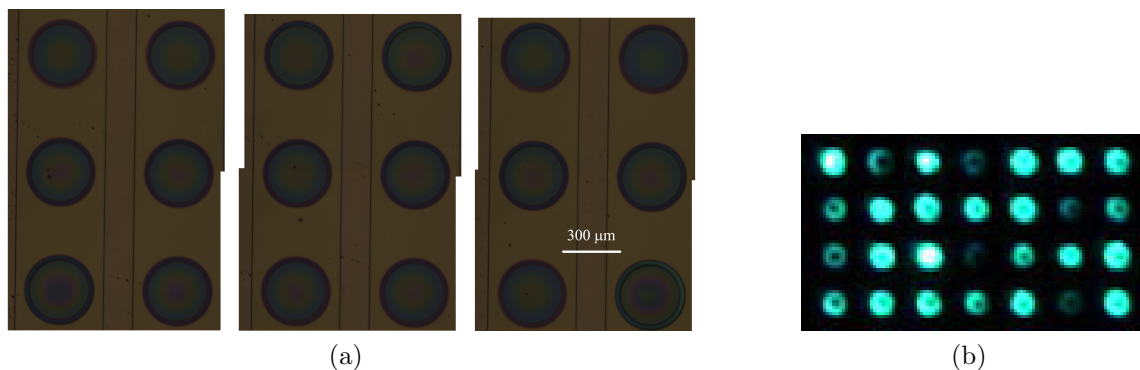


Figure 4.24: A passive matrix OLED display with light-emitting layer printed by the LAMP method. (a) An optical micrograph (combined) showing  $3 \times 6$  pixels after the printing of PVK+PBD+C6 layers. Vertical stripes shown are ITO anodes. Horizontal cathode stripes will be deposited later. (b) A  $4 \times 7$  array under test.

## 4.6 Summary

In summary, we introduced the LAMP method to deposit organic light emitting materials for full-color OLED application. We discussed the method we used to selectively pattern the wettability of the printing plate and the printing apparatus built to do the printing operation, including the laser alignment system. Both single-color arrays and RGB arrays have been demonstrated, with either slow-evaporation-rate solvents or a volatile solvent. In addition, working devices with printed light-emitting layers have been shown, with performance comparable to spin-coated control devices. A passive matrix OLED display has also been fabricated. Based on its large-area and low-cost capability, we believe that this novel patterning method has great potential in future applications. However, the non-uniformity of the film thickness needs to be optimized, which will be discussed in Chapter 5.